The Henryk Niewodniczański
INSTITUTE OF NUCLEAR PHYSICS
Polish Academy of Sciences
ul. Radzikowskiego 152, 31-342 Kraków, Poland

www.ifj.edu.pl/publ/reports/2011/

Kraków, February 2011

Report No. 2048/PS

THE APPLICATION OF SELECTED NEUTRON SCATTERING TECHNIQUES TO THE STUDY OF SHORT RANGE ORDER IN SOFT MATTER

Wojciech Zając

Habilitation Thesis

Acknowledgements

I would like to express my appreciation towards Professor Jerzy Janik, who once invited me to his group and for life "infected" with the beauty and elegance of neutron scattering studies of molecular matter. His advice and guidance have been invaluable.

I acknowledge the encouragement of my superiors, my colleagues and friends from the Henryk Niewodniczański Institute of Nuclear Physics Polish Academy of Sciences. Exceptionally friendly and motivating atmosphere they have been always creating is a landmark of this Institute and make working here an honour and a pleasure.

Special thanks are due to my partners at many neutron scattering projects: Dr Barbara Gabryś from Oxford University and Professor Otto Schärpf, now retired expert in polarized neutron scattering, and the father of the D7 instrument at the ILL, Grenoble.

My research would never be possible without loving encouragement and patience of my dear wife Milena, to whom I dedicate this work.

Preface

In this work soft matter is represented by polymers: substances of considerable, multilevel structural complexity. Through describing results obtained in course of a number of research projects, both published and unpublished, this report presents several neutron scattering techniques applicable in the study of short range order in soft matter. Among these techniques one is well known and routinely used: Small Angle Neutron Scattering (SANS). However, the report focuses on relatively rarely exploited methods, requiring rare instrumentation and a lot of effort in data analysis, first of all on diffuse scattering of polarized neutrons with polarization analysis. Chapter 6 illustrates this method at work, starting from a simple proof that short range order is partly destroyed in miscible polymer blends and ending on co-operation of diffuse scattering and small angle scattering in revealing spatial correlations in ionomer networks. An example of the application of diffuse scattering of polarized neutrons to solving a practical problem in applied materials science makes Chapter 7. To the author's knowledge, this is the only such experiment known in literature.

Some inelastic neutron scattering techniques have also been counted among those probing local order, although indirectly. Indeed, in many soft matter systems, particularly in liquid crystals, quasielastic neutron scattering (QENS) is a powerful source of information on the coupling between stochastic molecular dynamics and their polymorphism [1-5].

The last chapter shortly mentions two "exotic" techniques: SANS under zero average contrast condition (ZAC) and deep inelastic (Compton) scattering. Experimental material illustrating these techniques did not reach far beyond test measurements and feasibility studies. Anybody attempting this type of experiments as a typical user of large scale research facilities, faces bidding for beam time via a procedure of submitting proposals to selection panels that operate on the peer-review principle. Consequently, competing proposals that guarantee leading-edge

publishable results at the cost of much less beam time are nearly always the winners. The fact that both experiments described in Chapter 9 were found interesting and ambitious, and finally got the green light, although in case of ZAC-SANS the time allocated was order of magnitude less than needed, justifies the space they take in this report.

Theoretical and descriptive introductory parts are kept to absolute minimum, needed for clarity of the main text. The choice of particular issues covered in these parts has been driven by the author's subjective opinion of what is a worth mentioning. For example, the origin of coherent and incoherent scattering lengths for a single nucleus, the importance of understanding multiple scattering effects or how the neutron beam can be polarized are shortly treated.

Neutron scattering techniques are expensive and not available at the asking. They are called when none of simpler ones can do the job. This is why samples subjected to neutron experiments must have been thoroughly investigated by other methods, especially "desktop" ones (such as DSC). This principle is illustrated here by choosing polymers and their modifications that are known with respect to their physical and chemical properties.

Contents:

1 Introduction

1.1 Key to symbols and abbreviations

1.1.1 List of symbols

ϑ	Scattering angle (the angle between the incidence direction and the reflecting plane)
θ	The angle between the incidence direction and the scattering direction ($\theta = 2\,\vartheta$)
Φ	Neutron flux
$\mathbf{J}$	Neutron current
$\mathbf{k}$, k	Wave vector and its modulus
$\mathbf{Q}$, Q	Wave vector transfer (scattering vector) and its modulus
$\mathbf{q}$, q	Momentum transfer and its modulus
μ	Effective mass
$V^*(r)$	The Fermi pseudopotential
σ	Scattering cross section, measured in barns. 1 barn = 10^{-24}cm^2 = 10^{-28}m^2
A	The "zero-angle scattering" (SANS, Debye-Bueche model)
a	Distance parameter
a_c	correlation length (SANS, Debye-Bueche model)
$\hat{B}$	Scattering length operator
D_f	Fractal dimension (in SANS scattering law)

d	Characteristic spacing (in the context of diffraction)
b	Scattering length
$\left\|F(\mathbf{Q})\right\|^2$	Particle form factor (in SANS)
$G(r)$	Radial distribution function, also particle-particle correlation function (in SANS)
$G_s(\mathbf{r},t)$	Self-correlation function
$\chi_{1,2}$	Interaction parameter (theory of mixing)
ϕ	Composition (of a blend)
φ	The volume fraction
FWHM	Full width at half maximum
G_m , ΔG_{mix}	Gibbs free energy of mixing
I	Nuclear spin
$I(Q)$	Scattering intensity
$I_{inc}(\mathbf{Q},t)$	Intermediate scattering function
$J(Y)$	Compton profile
N	Number density of nuclei
n	Refractive index
$\mathbf{s}$	Nuclear spin vector
$\mathbf{P}_{\text{in}}$, $\mathbf{P}_{\text{out}}$	Beam polarization (incoming, outgoing)
R	Flipping ratio, also the radius (by general convention)
R_g	Radius of gyration
$S(Q)$	Structure factor (in SANS)
$\rho(\mathbf{r})$	Scattering length density
ξ	System-characteristic length scale (in SANS scattering law)

1.1.2 List of abbreviations

DSC	Differential scanning calorimetry
EISF	Elastic Incoherent Structure Factor
PBT	Poly(butylene terephthalate)
PEO	Poly(ethylene oxide)
PMMA	Poly(methyl metacrylate)
PC	Polycarbonate (bisphenol-A-polycarbonate)
PS	Polystyrene
QENS	Quasielastic Neutron Scattering
SALS	Small Angle Light Scattering
SANS	Small Angle Neutron Scattering
SAXS	Small Angle X-Ray Scattering
SLD	Scattering length density
SPBT	Sulphonated poly(butylene terephthalate)
SPS	Sulphonated polystyrene
UCST	Upper critical solution temperature
WANS	Wide Angle Neutron Scattering
ZAC-SANS	Small Angle Neutron Scattering under Zero Average Contrast Condition

1.2 Properties of the neutron and naming conventions

Properties of the neutron

Quantity	Symbol	Value
Rest mass	m_n	1.674927211(84) x 10^{-27} kg
	m_n	1.00866491597(43) at.u.
	$m_n c^2$	939.565346(23) MeV
Spin	I	½
Charge		0
Magnetic moment	μ_n	-0.96623641·10^{-27} J·T
	μ_n	-1.0418756272·10^{-3} μ_B
Mean life time (free)	τ	879.9±0.9 s (very recent value by [6])

(Numerical values used for calculations after [7])

Useful relations

Particle properties Energy – momentum relations:	Wave properties Frequency – wavelength relations
$E = \frac{m_n v^2}{2}; \quad E = \frac{p^2}{2m_n}; \quad p = m_n v$	$E = \hbar\omega = \frac{\hbar^2 k^2}{2m_n}; \quad p = \hbar k; \quad k = \frac{2\pi}{\lambda}$

$$E[\text{meV}] = 81.804 \cdot \lambda^{-2}[\text{Å}^{-2}] = 0.81804\lambda^{-2}[\text{nm}^{-2}]$$

$$E[\text{meV}] = 0.0207212 \cdot k^2[\text{nm}^{-2}] = 2.07212 \cdot k^2[\text{Å}^{-2}]$$

$$\lambda[\text{nm}] = \frac{395.6}{v[\text{m/s}]} \qquad \lambda[\text{Å}] = \frac{3956}{v[\text{m/s}]}$$

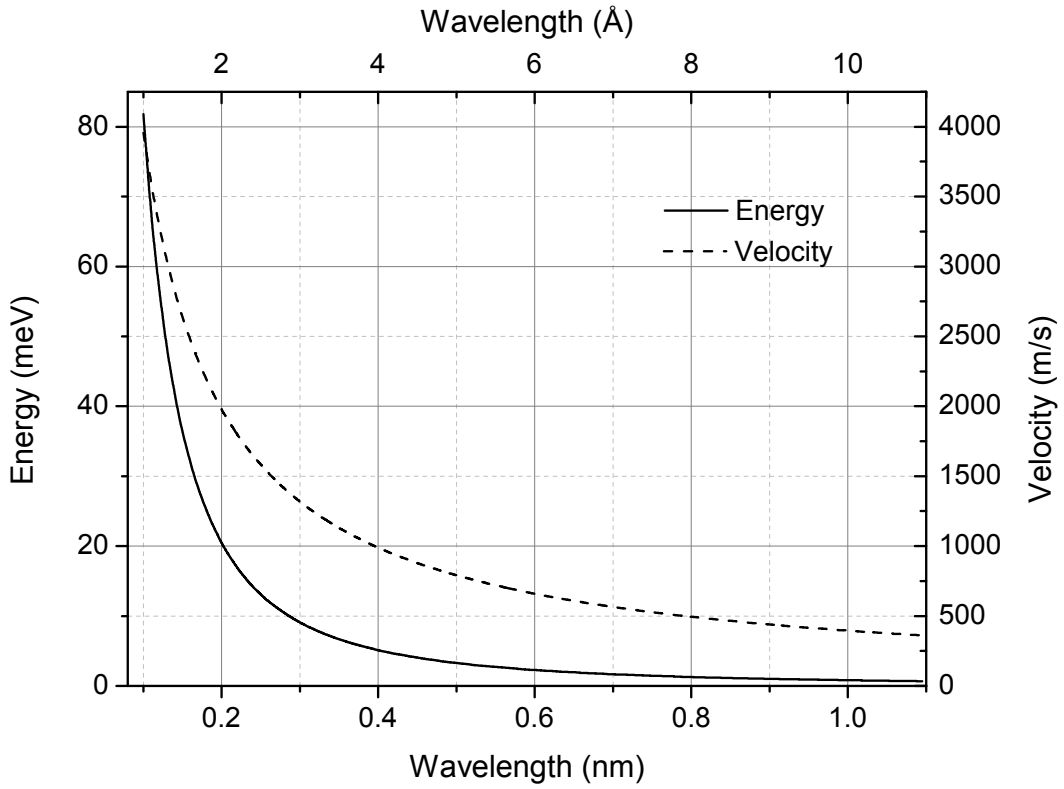

Fig. 1-1.Neutron wavelength – energy – velocity relation.

A generally accepted classification with respect to *neutron temperature,* i.e. free neutron's kinetic energy (various sources may give slightly different classification borders):

Energy [meV]	**Wavelength** [Å]	[nm]	**Energy classification**
$< 3\cdot10^{-4}$	> 520	> 52	ultra cold
$3\cdot10^{-4} \div 0.05$	40 ÷ 520	4 ÷ 52	very cold
0.05 ÷ 10	3 ÷ 40	0.3 ÷ 4	cold
10 ÷ 100	0.9 ÷ 3	0.09 ÷ 0.3	thermal
100 ÷ 500	0.4 ÷ 0.9	0.04 ÷ 0.09	hot
500 ÷ 10^5	0.03 ÷ 0.4	$3\cdot10^{-3} \div 0.04$	epithermal
< 400	> 0.5	<0.05	slow
> 1000	< 0.3	> 0.03	fast
< 1000	> 0.3	< 0.3	low energy region
1000 ÷ 10^7	$3\cdot10^{-3} \div 0.03$	$3\cdot10^{-4} \div 3\cdot10^{-3}$	resonance region
$10^7 \div 2.5\cdot10^{10}$	$5\cdot10^{-5} \div 3\cdot10^{-3}$	$5\cdot10^{-6} \div 3\cdot10^{-4}$	continuum region

Assuming that the neutrons emerging from the source are in thermal equilibrium with the moderator kept at the desired temperature, their flux is described by the Maxwellian distribution [8]:

$$\Phi(E)\,dE = \Phi_0 \frac{2}{\pi} \frac{\sqrt{E}}{(k_B T)^{3/2}} \exp\left(-\frac{E}{k_B T}\right) dE \tag{1.1}$$

This is shown in Fig. 1-2 for temperatures corresponding to four typical moderators. Contemporary neutron sources have various moderatos installed to suit specific needs, and such that they can cope with extreme working conditions. The actual flux at the beam exit ports may therefore differ due to particular moderating properties of a given substance.

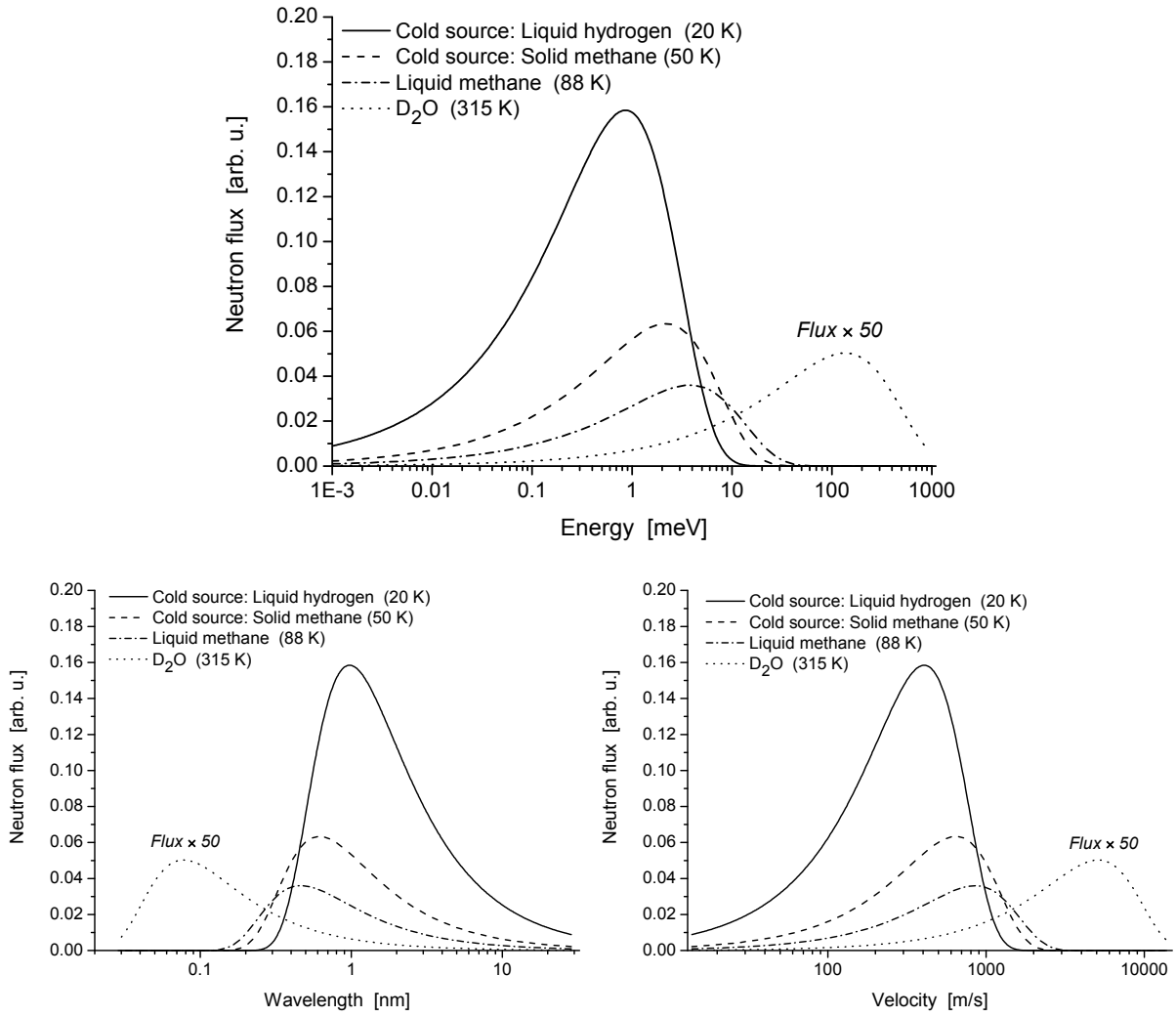

Fig. 1-2. Neutron flux distribution as a function: neutron energy, neutron wavelength and neutron velocity for typical moderator temperatures.

1.3 The scattering geometry

Schematic representation of the scattering geometry concludes the introductory chapter on naming conventions.

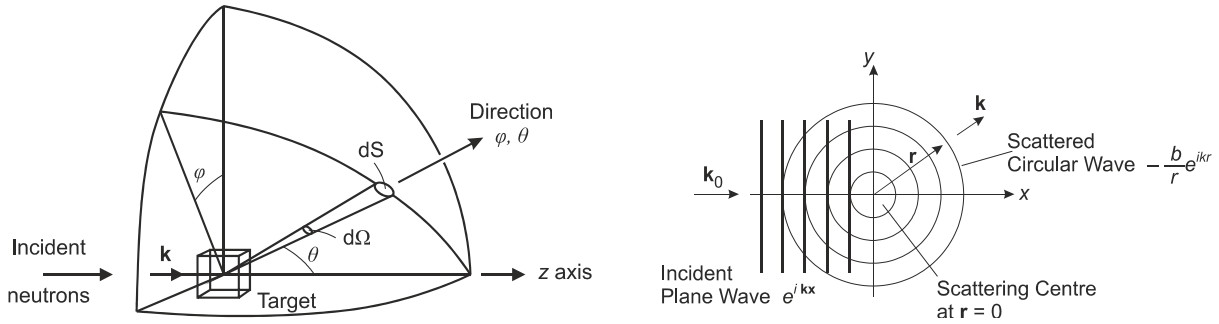

Fig. 1-3. Schematic representation of the scattering geometry.

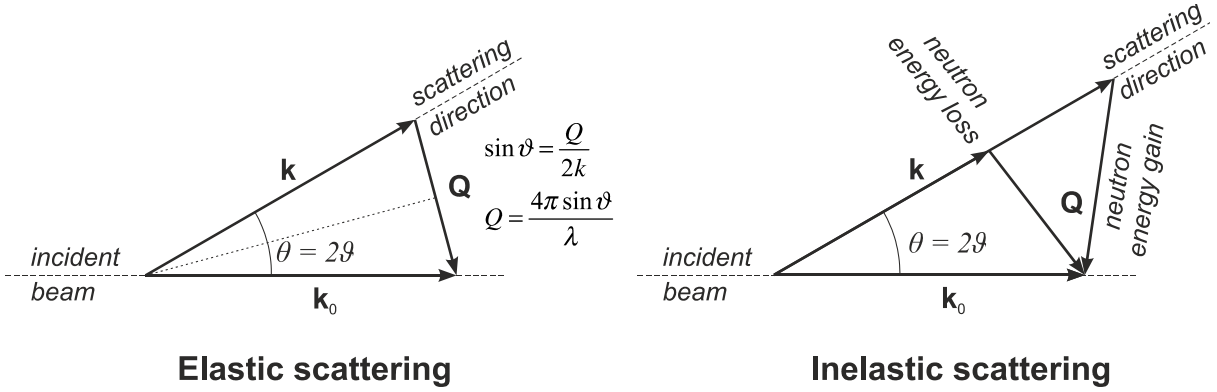

Fig. 1-4. "Scattering triangles" for elastic and inelastic events.

The angle between the incident and scattering directions is usually denoted 2θ, as in the case of reflection from a crystal plane it is twice the scattering angle between the incident (or reflected) beam and the plane in question.

On the other hand, the same angle between the incident and scattering directions is the polar angle (colatitude) in the spherical system of coordinates (z-axis pointing towards the incident direction). In this case it is denoted by θ.

In order to avoid confusion, in this work the scattering angle is denoted by ϑ, while the colatitude receives the θ symbol.

2 Theoretical introduction

2.1 Basic formulae

Theory of neutron scattering is covered in detail in a number of worldwide known texts (see e.g. [8-11]) and numerous review articles, reports and study monographs[1]. Here, some principles are outlined that are relevant to the analysis of scattering from soft and partially disordered matter, with the emphasis on an application of scattering of polarised neutrons with spin polarisation analysis.

Theoretical treatment of neutron scattering usually starts with the quantum mechanical description of a two-body collision. The incident beam is represented by a travelling plane wave:

$$\Psi_{in} = ae^{i\left(\vec{k}\cdot\vec{r}-\omega t\right)}. \tag{2.1}$$

Here a is determined by normalization condition. The scattered wave, which results from the interaction in the region of the centrosymmetric potential $V(r)$, takes the form of an outgoing spherical wave:

$$\Psi_{sc} = f(\theta)a\frac{e^{i(kr-\omega t)}}{r}, \tag{2.2}$$

where $f(\theta)$, which has the dimension of length, denotes the amplitude of scattering in the direction of angle θ relative to the direction of incidence (see Figs 1-3 and 1-4).

In order to describe the scattering process quantitatively, it is most convenient to define the cross section via the scattering amplitude and then to work out the latter (cf. e.g. [8,12]). Given the

[1] Excellent lecture handouts from e.g.

- Summer School on the Fundamentals of Neutron Scattering, NIST Center for Neutron Research
- National School on Neutron & X-ray Scattering, Oak Ridge National Laboratory
- The Jülich Centre for Neutron Science (JCNS) Laboratory Course - Neutron Scattering

particles in state Ψ, their current density **J**, being the number of particles of mass *m* passing through a perpendicular unit area in unit time is defined by:

$$\mathbf{J} = \frac{-i\hbar}{2m}\left[\Psi^*\nabla\Psi - \Psi\nabla\Psi^*\right] \tag{2.3}$$

For the incident beam this, together with (2.1), gives:

$$J_{in} = va^2; \quad v = \frac{\hbar k}{\mu}, \tag{2.4}$$

where v is the speed of an effective particle of mass μ. The number of particles per second scattered through an element of surface area $d\Omega$ about the direction **Q** on a unit sphere, is expressed through the scattered flux:

$$\left(\mathbf{J}_{sc}\cdot\mathbf{\Omega}\right)d\Omega = v\left|f\left(\theta\right)\right|^2 d\Omega\,. \tag{2.5}$$

Now the corresponding angular differential cross section takes the form:

$$\frac{d\sigma\left(\theta\right)}{d\Omega} = \frac{\mathbf{J}_{sc}\cdot\mathbf{\Omega}}{J_{in}} = \left|f\left(\theta\right)\right|^2. \tag{2.6}$$

This is the fundamental expression relating the scattering amplitude to the cross section. The task of calculating the scattering amplitude is then accomplished through the formal solution of the Schrödinger equation, and finally through taking the first Born approximation.

In the Born approximation the scattering amplitude is given by the Fourier transform of the interaction potential (see Fig. 2-1):

$$f\left(\theta\right) = -\frac{2\mu}{4\pi\hbar^2}\int d^3r e^{i\mathbf{Q}\cdot\mathbf{r}}V\left(r\right) \quad \text{with} \quad \mathbf{Q}\equiv\mathbf{k}-\mathbf{k}_0. \tag{2.7}$$

The Fourier transform variable **Q** is a wave vector, the difference between the wave vectors of the scattered and incident waves **k** and $\mathbf{k}_0$, respectively. It is referred to as the *wave vector transfer* or the *scattering vector.* In the neutron scattering *jargon,* one often finds the term "momentum transfer" applied to the vector **Q** or to its modulus. Although formally incorrect, it is nevertheless

understood unambiguously. Momentum transfer (in this report denoted by *q*) is related to the scattering vector via the Plank's constant:

$$Q = \frac{q}{\hbar}. \tag{2.8}$$

For an elastic scattering $\left(|\mathbf{k}| = |\mathbf{k}_0|\right)$, the magnitude of the scattering vector is given by:

$$|\mathbf{Q}| \equiv Q = 2k_0 \sin\frac{\theta}{2} \equiv k_0\sqrt{2\left(1-\cos\theta\right)}. \tag{2.9}$$

Therefore, in the Born approximation the dependence on the scattering angle enters through the wave vector transfer.

The simplicity of the result of the Born approximation makes it widely useful. The theory of thermal neutron scattering depends critically on the use of this approximation.

However, strictly speaking the condition for the validity of the Born approximation with the "true" interaction potential is not fulfilled in the case of thermal neutron scattering. This was first noticed and solved by E. Fermi. The Fermi's idea involves the introduction of a pseudopotential in place of the actual neutron-nucleus interaction. The fictitious Fermi potential $V^*(r)$, or pseudopotential, has the well depth and range scaled so that $V^*(r)$ is a spherical well with depth V_0^* and range r_0^*. In other words, the suggestion of Fermi was in effect to distort the neutron-nucleus interaction by extending the range and decreasing the depth in such a way that the transformation preserves the scattering length, namely:

$$V^*(r) = \frac{2\pi\hbar^2}{m} b\delta(r) \tag{2.10}$$

A virtue of Eq. (2.10) is that the correct scattering cross section is already built into the potential. In general, b is a complex number: $b = b' - ib''$. Since it refers to the fixed nucleus, it is called the bound scattering length. In the low-energy limit the scattering (s-wave) cross section and the absorption cross section far form resonant capture are given by:

$$\sigma_s = 4\pi |b|^2 ; \quad \sigma_a = \frac{4\pi}{k_0} b'' \tag{2.11}$$

2.2 Separation of coherent and incoherent cross sections

Given an ensemble of nuclei, we may combine (2.6) and (2.7) to calculate the differential cross section:

$$\frac{d\sigma(\theta)}{d\Omega} = |f(\theta)|^2 = \left(\frac{2\mu}{4\pi\hbar^2}\right)^2 \left|\left\langle \int d^3 r e^{i\mathbf{Q}\cdot\mathbf{r}} V^*(r) \right\rangle\right|^2 , \tag{2.12}$$

where $\langle \ldots \rangle$ indicates the ensemble average. For each nucleus, its scattering length b_i can be expressed in terms of the ensemble average $\langle b \rangle$ separated out:

$$b_i = \langle b \rangle + \delta b_i . \tag{2.13}$$

Then, after substitution of the explicit expression for $V^*(r)$ and a few algebraic transformations, one arrives at:

$$\frac{d\sigma(\theta)}{d\Omega} = \langle b \rangle^2 \sum_{i,j} \left\langle \exp\left(i\mathbf{Q}\mathbf{r}_{ij}\right) \right\rangle + \sum_i \left(\delta b_i\right)^2 \equiv \left[\frac{d\sigma(\theta)}{d\Omega}\right]_{coh} + \left[\frac{d\sigma(\theta)}{d\Omega}\right]_{inc} , \tag{2.14}$$

i.e. at the formula expressing $\frac{d\sigma(\theta)}{d\Omega}$ in terms of coherent and incoherent components. Here $\mathbf{r}_{ij} = \mathbf{r}_i - \mathbf{r}_j$ denotes the relative position of nucleus *j* with respect to nucleus *i*.

Both coherent and incoherent processes contribute to the total scattering. There are two sources of incoherence: the isotope incoherence and the spin incoherence. The former arises from the presence of different isotopes of the same element in an ensemble of nuclei, whereas the latter is due to various possible mutual orientations of neutron and nuclear spins. For an ensemble of nuclei, the isotope incoherent and the spin incoherent contributions to the incoherent scattering $\overline{b^2} - \left(\overline{b}\right)^2$ are expressed by:

$$\overline{b^2}-\left(\bar{b}\right)^2 = \underbrace{\left\langle\left(\bar{b}\right)^2\right\rangle-\left(\bar{b}\right)^2}_{\text{isotope incoherent}} + \underbrace{\frac{1}{3}B^2I\left(I+1\right)}_{\text{spin incoherent}} \tag{2.15}$$

If the target nucleus has a non-zero spin then the neutron and nuclear spins could be either parallel or antiparallel during the scattering process. The neutron, being a fermion with spin ½, couples to the nuclear spin I to give:

- $2\left(I+1\right)$ degenerate states for the eigenvalue of $I+\frac{1}{2}$, corresponding to parallel arrangement of the neutron and nucleus spins, with the scattering length conventionally denoted by b_+,
- $2I$ degenerate states for the eigenvalue of $I-\frac{1}{2}$, corresponding to antiparallel arrangement of both spins. The related scattering length is denoted by b_-.

Therefore there are altogether $2\left(2I+1\right)$ states with the following relative weights:

$$W_+=\frac{2I+2}{2\left(2I+1\right)}=\frac{I+1}{2I+1} \quad \text{and} \quad W_-=\frac{2I}{2\left(2I+1\right)}=\frac{I}{2I+1}; \quad W_++W_-=1 \tag{2.16}$$

Coherent scattering length is the weighted average of b_+ and b_-, while incoherent scattering length is given by the variance of b_+ and b_-:

$$b_c=W_+b_++W_-b_-; \quad b_i^2=W_+W_-\left(b_+-b_-\right)^2 \tag{2.17}$$

The corresponding cross sections are (cf. (2.11)):

$$\sigma_c=4\pi b_c^2 \quad \text{and} \quad \sigma_i=4\pi b_i^2 \tag{2.18}$$

Coherent scattering is *Q*-dependent and therefore it contains structural information.

In the case of hydrogen, (^{1}H) the following numerical values have been measured [13,14]:

b_+ = 10.817(5) fm, b_- = –47.420(14) fm, hence: b_c = –3.7406 fm, b_i = 25.274 fm, σ_c = 1.7583 barn, σ_i = 80.27 barn. It is now clear that doing neutron experiments with

hydrogen-rich samples one deals with predominant incoherent scattering. Neutron diffraction on well-ordered materials does not suffer very much from incoherent background which can be estimated and subtracted leaving "pure" Bragg peaks with good enough counting statistics. Nevertheless, a serious difficulty arises when disordered samples are under consideration, i.e. when attention is focused on short-range order (spatial correlations of the order of 1 nm), and isotopic substitution (hydrogen – deuterium) is either impossible or undesirable. In this case a polarized neutron beam can be used with polarization analysis of the scattered neutrons [15]. A comprehensive coverage of this subject can be found in [16] and references therein. In what follows, the principles of the method are briefly outlined (cf. [17,18]).

Let I be the non-zero nuclear spin and let b_+ and b_- denote scattering lengths associated with the $I+\frac{1}{2}$ and $I-\frac{1}{2}$ compound states of the nucleus-neutron system. Let $\hat{B}$ denote the scattering length operator. Then b_+ and b_- are its eigenvalues. It can be shown that (cf. [8]):

$$\hat{B} = \bar{b} + \frac{1}{2} b_N \, \hat{\sigma} \cdot \hat{I} \, . \tag{2.19}$$

Here $\hat{\sigma}$ is the Pauli spin operator and $\hat{I}$ is the nuclear spin operator. $\bar{b}$ and b_N are expressed in terms of b_+ and b_- through:

$$\bar{b} = \frac{(I+1)b_+ + Ib_-}{2I+1} \quad \text{and} \quad b_N = \frac{2(b_+ - b_-)}{2I+1} \tag{2.20}$$

Further calculations are carried out by means of the density matrix formalism, and lead to the expression for the differential nuclear scattering cross-section (refs. [16,17] and references therein):

$$\frac{d\sigma}{d\Omega} = Tr\left[\rho \hat{B}^{\dagger} \left(\hat{\sigma} \cdot \hat{I}^{\dagger} \right) \hat{B} \left(\hat{\sigma} \cdot \hat{I} \right) \right] \tag{2.21}$$

Let $\mathbf{s}_n$ denote the spin vector of an individual ("n-th") neutron in the ensemble $\left(|\mathbf{s}_n| = 1/2 \right)$, and then let us define the beam polarization $\mathbf{P}$ as the ensemble average over all the neutron spin vectors, normalised to their modulus:

$$\mathbf{P} = \frac{\langle \mathbf{s}_n \rangle}{1/2} = 2 \langle \mathbf{s}_n \rangle \tag{2.22}$$

In the presence of an external field, providing the natural quantization axis, the beam polarization becomes a scalar value:

$$P = \frac{N_+ - N_-}{N_+ + N_-}, \tag{2.23}$$

where N_+ and N_- are the number of neutrons with spin-up and spin-down with respect to the field direction. Let us take this opportunity to define the so called *flipping ratio, R,* a measurable quantity we will refer to later in the next chapter:

$$R = \frac{N_+}{N_-} \tag{2.24}$$

Using definition (2.24), the expression (2.23) becomes:

$$P = \frac{R-1}{R+1} \tag{2.25}$$

Now the differential cross section (2.21) can also be expressed as a function of incoming beam polarization $\mathbf{P}^{(in)}$:

$$\frac{d\sigma}{d\Omega} = \hat{B}\hat{B}^{\dagger}\left[I(I+1) + i\mathbf{P}^{(in)}\left(\hat{I}^{\dagger} \times \hat{I}\right)\right] \tag{2.26}$$

If nuclear spins are unpolarized, which is normally the case, averaging over nuclear spin orientations must be performed. Then, after taking into account the properties of the nuclear spin operator and $\hat{I}$ one obtains for the differential cross section [16]:

$$\frac{d\sigma}{d\Omega} = \hat{B}^{\dagger}\hat{B}I(I+1), \tag{2.27}$$

and for the scattered polarization:

$$P_{\gamma}^{(out)}\frac{d\sigma}{d\Omega} = Tr\left[\rho\hat{B}^{\dagger}\left(\hat{\sigma}\cdot\hat{I}^{\dagger}\right)\sigma_{\gamma}\left(\hat{\sigma}\cdot\hat{I}\right)\hat{B}\right], \tag{2.28}$$

where the index γ denotes a particular direction in space. Again, evaluation of the right-hand side of Eq. (2.28), followed by averaging over nuclear spin orientation, gives [16]:

$$P_{\gamma}^{(out)}\frac{d\sigma}{d\Omega} = -\frac{1}{3}P^{(in)}I(I+1)\hat{B}^{\dagger}\hat{B} \tag{2.29}$$

Let us introduce the conventional notation $I^{\uparrow\downarrow}$ and $I^{\uparrow\uparrow}$ for the scattered intensity with and without the spin flip. Then by definition:

$$\frac{d\sigma}{d\Omega} = I^{\uparrow\uparrow} + I^{\uparrow\downarrow} = I_\gamma^{\uparrow\uparrow} + I_\gamma^{\uparrow\downarrow} \tag{2.30}$$

and:

$$P_\gamma^{(out)} \frac{d\sigma}{d\Omega} = \frac{I_\gamma^{\uparrow\uparrow} - I_\gamma^{\uparrow\downarrow}}{I_\gamma^{\uparrow\uparrow} + I_\gamma^{\uparrow\downarrow}} \left(I_\gamma^{\uparrow\uparrow} + I_\gamma^{\uparrow\downarrow} \right) = I_\gamma^{\uparrow\uparrow} - I_\gamma^{\uparrow\downarrow} \tag{2.31}$$

Combining Eqns. (2.27) and (2.31) gives:

$$\frac{d\sigma}{d\Omega} = I^{\uparrow\uparrow} + I^{\uparrow\downarrow} = \hat{B}^\dagger \hat{B} I\left(I+1\right) \tag{2.32}$$

and:

$$P_\gamma^{(out)} \frac{d\sigma}{d\Omega} = \frac{I_\gamma^{\uparrow\uparrow} - I_\gamma^{\uparrow\downarrow}}{I_\gamma^{\uparrow\uparrow} + I_\gamma^{\uparrow\downarrow}} \left(I_\gamma^{\uparrow\uparrow} + I_\gamma^{\uparrow\downarrow} \right) = I_\gamma^{\uparrow\uparrow} - I_\gamma^{\uparrow\downarrow} = -\frac{1}{3} \hat{B}^\dagger \hat{B} I\left(I+1\right) \tag{2.33}$$

Finally:

$$I^{\uparrow\uparrow} = \frac{1}{3}\left|B\right|^2 I\left(I+1\right), \qquad \text{and:} \qquad I^{\uparrow\downarrow} = \frac{2}{3}\left|B\right|^2 I\left(I+1\right). \tag{2.34}$$

Thus the outgoing scattering intensity from unpolarized nuclear spins is always one third without, and two thirds with flip of the neutron spin from the polarized beam.

The coherent scattering I_{coh} and incoherent scattering I_{inc} are linearly related to the measured spin-flip and non-spin-flip scattering [8]:

$$I_{coh} = I^{\uparrow\uparrow} - \frac{1}{2} I^{\uparrow\downarrow} \quad \text{and} \quad I_{inc} = \frac{3}{2} I^{\uparrow\downarrow}. \tag{2.35}$$

Total scattering is a sum of the two. In this way, shining a polarized neutron beam upon the sample and separately recording neutrons scattered with their spin conserved and with spin flipped, the experimenter can separate coherent from incoherent scattering right at the instrument level.

3 Experimental diffuse scattering of polarized neutrons with polarization analysis

3.1 Polarizing a neutron beam

There are three types of neutron polarizers in general use, all of them having their advantages in particular types of experiments [19]:

1. Polarizing crystals (e.g. $Co_{92}Fe_8$, Heusler crystals (Cu_2MnAl)) using preferential Bragg reflection),
2. Polarizing mirrors and supermirrors, (using preferential reflection from a set of alternating magnetic and non-magnetic layers of increasing thickness) usually arranged so that they resemble Soler slits, and slightly bent to ensure reflection under a very small angle for each passing neutron, [20,21],
3. Polarizing filters (e.g. preferential absorption by polarized ^{3}He nuclei) [20,22-24].

ad 2.: The operation of this type of neutron polarizer relies on the spin dependence of the refractive index $n = \frac{\lambda_1}{\lambda_2} = \frac{k_2}{k_1}$:

$$n_{\pm} = 1 - \left(\frac{N\lambda^2}{2\pi} \right) \left(\bar{b} \pm \bar{p} \right), \tag{3.1}$$

where N is the number density of scattering nuclei, and $\bar{b}$ and $\bar{p}$ are the parameters of the Fermi pseudopotential for nuclear and magnetic scattering (cf. Eq. (2.10)) [25]:

$$\left\langle V^*_{Nucl} \right\rangle = \frac{2\pi\hbar^2}{m} N\bar{b} \quad \text{and} \quad \left\langle V^*_{Magn} \right\rangle = \frac{2\pi\hbar^2}{m} N\bar{p} \tag{3.2}$$

Expression (3.1) means that there are two critical angles for total external reflection (note that for neutrons usually $n < 1$):

$$\theta^{crit.}_{\pm} = \lambda \sqrt{\frac{N}{\pi} \left(\bar{b} \pm \bar{p} \right)} \tag{3.3}$$

The beam reflected between the two (very small) critical angles is fully polarized. The wavelength and N dependences in Eq. (3.3) imply that in practice magnetic multilayers must be prepared in order to ensure operation in a reasonable range of λ [25].

ad 3.: For a polarizing filter we define: σ_0 – spin-independent absorption cross section, and σ_p – spin-dependent absorption cross section. Then for the two possible spin states:

$$\sigma_{\pm} = \sigma_0 \pm \sigma_p \tag{3.4}$$

^{3}He nuclei are best suited for that polarizing filters, since for ^{3}He: $\sigma_0 = \sigma_p$, and hence only one spin state is transmitted through a filter with polarized ^{3}He.

3.2 The instrument

Diffuse coherent scattering experiments aimed at the study of short range order in polymers, reported here, were carried out on the D7 instrument at the Institute Laue-Langevin in Grenoble, whose layout is shown in Fig. 3-1 [21,26].

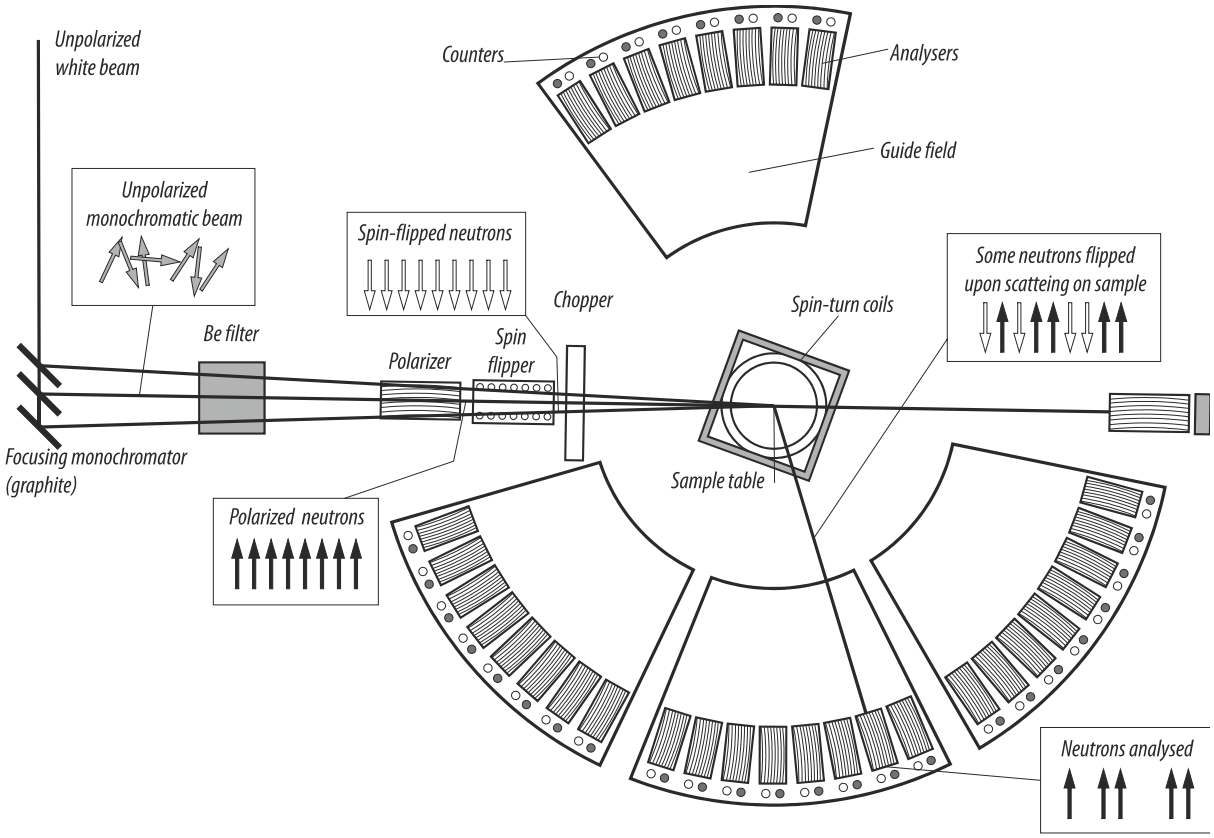

Fig. 3-1. Layout of the D7 diffuse neutron scattering instrument at the ILL, Grenoble

Monochromatized neutrons (λ = 0.312 nm, 0.4855 nm, 0.580 nm, or 3.12 Å, 4.855 Å , 5.8 Å) are passing through a polarizer on their way to the sample. Polarization analysers in front of the detectors are selecting neutrons with their spin direction identical to that after the polarizer. The weak guide field prevents neutron depolarization while travelling towards analysers.

Since such analysers have their analysing directions fixed in space, a "spin-flipper" is placed between the polarizer and the sample, and the instrument is operated in flip/non-flip alternating modes. The spin flipper (of Mezei type) is a coil with steady current so tuned that a neutron performs a half-period of Larmor precession on its way through it [27]. Although the device is very efficient, a correction for finite flipping ratio must be measured and included in data analysis. The flipping ratio is assessed by measuring a standard quartz sample which is an incoherent scatterer:

$$\begin{aligned} I_{corr}^{\uparrow\uparrow} &= I^{\uparrow\uparrow} - (R-1)^{-1}\left(I^{\uparrow\downarrow} - I^{\uparrow\uparrow}\right) \\ I_{corr}^{\uparrow\downarrow} &= I^{\uparrow\downarrow} + (R-1)^{-1}\left(I^{\uparrow\downarrow} - I^{\uparrow\uparrow}\right) \end{aligned} \tag{3.5}$$

Eq. (2.35) is then changed accordingly:

$$I_{coh} = I_{corr}^{\uparrow\uparrow} - \frac{1}{2} I_{corr}^{\uparrow\downarrow} \quad \text{and} \quad I_{inc} = \frac{3}{2} I_{corr}^{\uparrow\downarrow} \tag{3.6}$$

An important virtue of this method of direct measuring coherent scattering is that the latter can be normalized so that it is expressed in absolute units (e.g. barns per monomer per steradian). For this purpose the incoherent scattering intensity is used along with the calculated incoherent cross section per chemical unit (e.g. per monomer). Since in such experiments the incoherent scattering can be considered isotropic in space, we have [28]:

$$\frac{\partial \sigma_{coh}}{\partial \Omega} = \frac{\sigma_{inc}}{4\pi} \frac{I_{coh}}{I_{inc}} \tag{3.7}$$

Coherent scattering expressed in absolute units may prove helpful in the detailed study of certain semi-ordered systems (e.g. paracrystallinity in isotactic or syndiotactic polymers) [29]. It is also important to know the coherent scattering cross section when a reliable estimation of multiple

scattering is to be performed (see below). An example of relative contribution of the coherent and incoherent components to the total scattering is given in Fig. 3-2. The incoherent component has been corrected for the Debye-Waller factor. No multiple scattering corrections have been carried out for this example, what leads to significant background in the coherent component (see below). If such an experiment were performed without polarization analysis but with reliable estimation of the incoherent background, the details of coherent spectrum would be of the order of the resulting error bars of experimental uncertainty. In the example below the error bars are of the size of the point symbol.

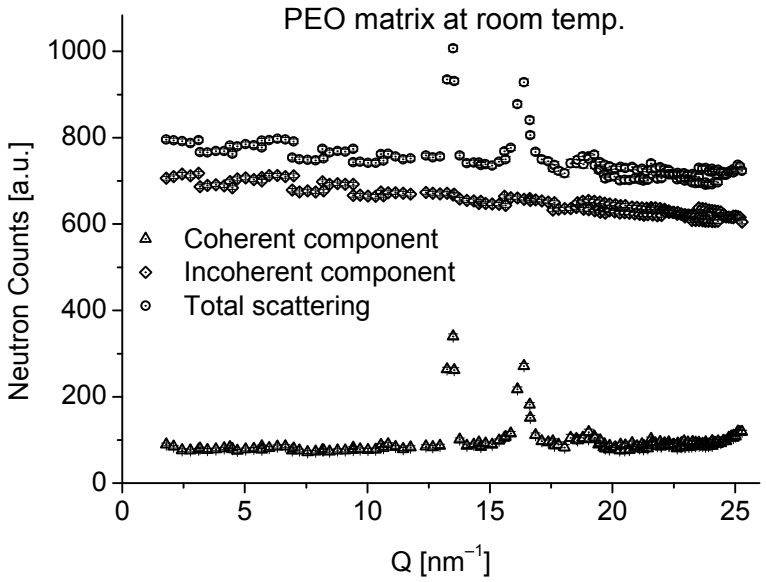

Fig. 3-2. An example of relative contributions of coherent and incoherent scattering in case of poly(ethylene oxide) [17].

3.3 Multiple scattering in diffuse scattering of polarized neutrons with polarization analysis

Theoretical considerations and model-building in the field of thermal neutron scattering usually rely on the implicit assumption that the neutron, once scattered by the sample nucleus, makes it towards the detector with no further interaction with other sample nuclei. Otherwise stated, it is assumed that the neutrons, whose wave vectors differ from initial values, registered by a detector, have exactly one scattering event in their history. This assumption is usually incorrect, and it depends on the particular experiment, whether this fact can be neglected or not. Consequently, approaches specific to particular fields of neutron scattering research have been developed, e.g.

for diffraction experiments [30], inelastic scattering [31,32], or deep inelastic (Compton) scattering [33]. Researchers have been aware of the problem of multiple scattering for more than half of a century [34], and carried out systematic experimental studies in this field ([35] and reference therein). It is tempting to accept that the "thinner" (in terms of beam transmission) the sample the better. However, the use of very thin samples results in poor signal-to-noise ratio and requires long measuring time. Moreover, extrapolation to zero thickness may not at all lead to plausible results [35], and the problem becomes more serious while working with flat samples.

A fairly coarse method of estimating the influence of double scattering in cylindrical samples (isotropic, elastic scattering) is due to Blech and Averbach ([36], also outlined in [37]) and consists in applying tabularized corrections to the experimental data.

Analytical formulae by Sears ([38], also outlined in [37]) allow one to calculate small multiple scattering correction for non-axially-symmetric samples, but they are by no means convenient or easy to implement.

It soon became apparent that the most versatile approach to multiple neutron scattering should rely on Monte Carlo "ray-tracing" calculations. Two well-known computer codes were then published nearly at the same time [39,40]. Out of these two, DISCUS by M. Johnson from Harwell [40] became the most widely used and the most frequently modified/tailored for particular needs, due to its high efficiency.

The idea of the separation of coherent and incoherent scattering relies on independent registration of neutrons with their spin flipped and those with their spin conserved. In real experiments, especially those with hydrogen-rich materials of non-negligible thickness, there is a significant probability of incoherent scattering on hydrogen nuclei, which always implies neutron spin flip. Consequently, there is quite a number of multiply scattered neutrons registered in the non-spin-flip channel that in fact never took part in coherent scattering.

Taking into consideration multiple scattering events, the spin-flip and spin-conserved scattering intensities will be "cross-populated", as schematically shown in Fig. 3-3:

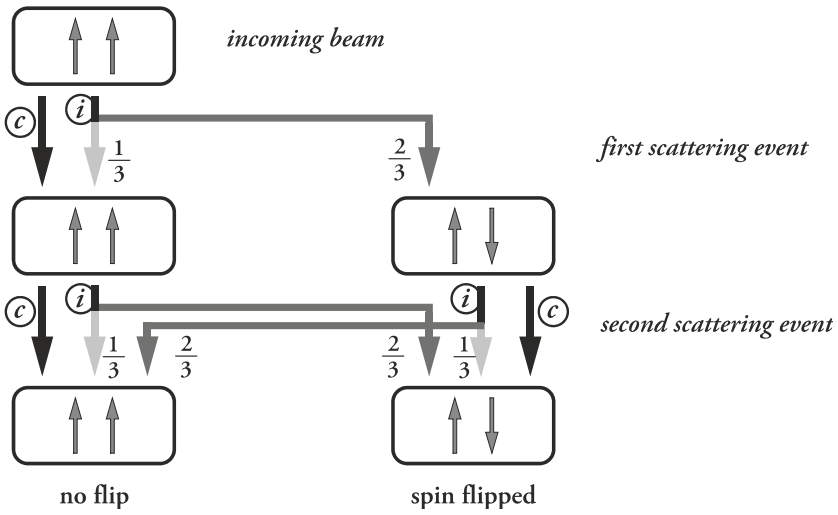

Fig. 3-3. Influence of multiple scattering upon population of spin-flip and non-spin-flip scattering intensities "c" stands for coherent scattering, and "I" for incoherent .

Although elastic incoherent scattering may, in first approximation, be considered isotropic (Q-independent), the coherent intensity is usually a rapidly varying function of Q. From Fig. 3-3 it is evident that multiple scattering will not only add a flat background to coherent intensity but in case of a thick or non-cylindrical sample will also modify the peak shapes [41].

In general, multiple scattering of neutrons can be approached through a set of transport equations describing scattering [34]:

$$\mathbf{s}\cdot\nabla P_n(\mathbf{r},\mathbf{s}) + \sigma_T P_n(\mathbf{r},\mathbf{s}) = \int d\Omega' \sigma_d(\mathbf{s},\mathbf{s}') P_{n-1}(\mathbf{r},\mathbf{s}'); \qquad n = 0,1,2,\ldots; \quad P_{-1} \equiv 0, \quad (3.8)$$

where $P_n(\mathbf{r},\mathbf{s})$ is the number of neutron per unit volume at **r**, which have already been scattered *n* times, and which are now proceeding in the direction of the unit vector **s**, $\sigma_d(\mathbf{s},\mathbf{s}')$ differential scattering cross section per unit volume, while scattering from direction **s** to **s**', $\sigma = \int \sigma_d d\Omega$ total scattering cross section per unit volume, integration over the solid angle 4π, and σ_T total scattering, including absorption. Although a format set of solutions to Eq. (3.8) exists [34], the only practical solution taking into account the sample shape, its real dimensions and the experimental geometry consists in Monte Carlo "ray-tracing" calculations. For this purpose a flagship code DISCUS implementing this method [40], was subsequently modified and adopted at the ILL for the interaction of neutron spin with nuclear spin, i.e. for experiments with neutron polarization analysis [37]. A comprehensive account of this subject is given by [41].

In order to illustrate real-life effects of multiple scattering, calculations have been performed assuming a previously measured differential coherent cross section for atactic polystyrene, expressed in terms of absolute units (barns per monomer per steradian). In Monte Carlo "ray-tracing" calculations both multiple scattering and self-extinction effects are treated simultaneously, as the distance travelled by a neutron inside the sample volume is correlated with the number of scattering events and the sample geometry.

Calculations have been carried out for two sample shapes: for a hollow cylinder of outer diameter of 20 mm, and for a slab 20×50 mm, placed under the angle of 45° to the initial beam direction. For each geometry, "thin sample" and "thick sample" cases were considered. The results are presented in Figs. 3-4 and 3-5. Abscissae represent the magnitude of scattering vector (wave vector transfer), while ordinates show scattering probabilities. For a slab sample, self-extinction makes certain scattering angles unusable. On the D7 instrument (see Fig. 3-1), these scattering angles can be covered by the use of the fourth detector bank, positioned as in Fig. 3-1.

The first rows in Figs. 3-4 and 3-5 compare "ideal" single scattering probabilities for hypothetical samples without self-absorption with "real" probabilities for samples with transmission calculated from their physico-chemical data. The second and third rows show contributions to apparent coherent scattering arising from double and triple scattering, respectively. In the fourth rows probabilities for single scattering are compared with apparent coherent scattering arising from the first four orders of scattering. The term "apparent coherent" refers to the formula (3.6) applied to the "spin-flip" and "non-spin-flip" intensities, cross-populated by multiple scattering as shown in Fig. 3-3.

In real-life treatment of experimental data, the true coherent cross-section as a function of Q is unknown. In fact, it is the quantity being sought in the measurement. This poses a problem if one wants to carry out multiple scattering corrections. A practical solution consists in first guessing this cross section from preliminary data analysis and taking it as a first approximation. The Monte Carlo program is then run, resulting in Q-dependent multiplicative corrections to $I^{\uparrow\uparrow}$ and $I^{\uparrow\downarrow}$. A corrected coherent cross section is then calculated and taken as the next approximation. If the first guess was good, then this iterative procedure converges after several steps. This route was successfully taken during data analysis in paper [18].

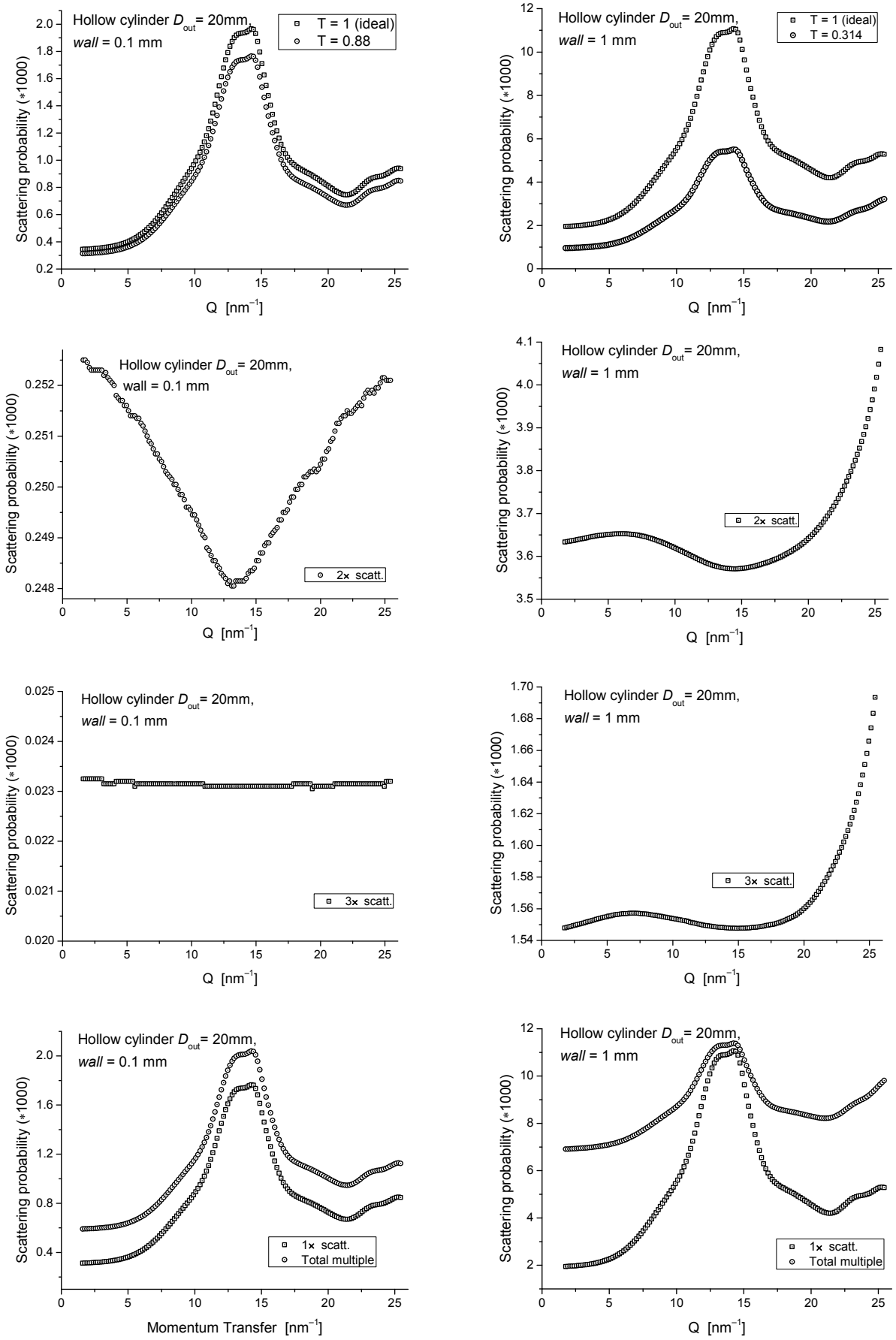

Fig. 3-4. Illustration of multiple scattering and self-extinction effects on coherent scattering from a hollow cylinder sample of atactic polystyrene. Left column: thin sample, right column: thick sample. Unpublished results. More explanation in text.

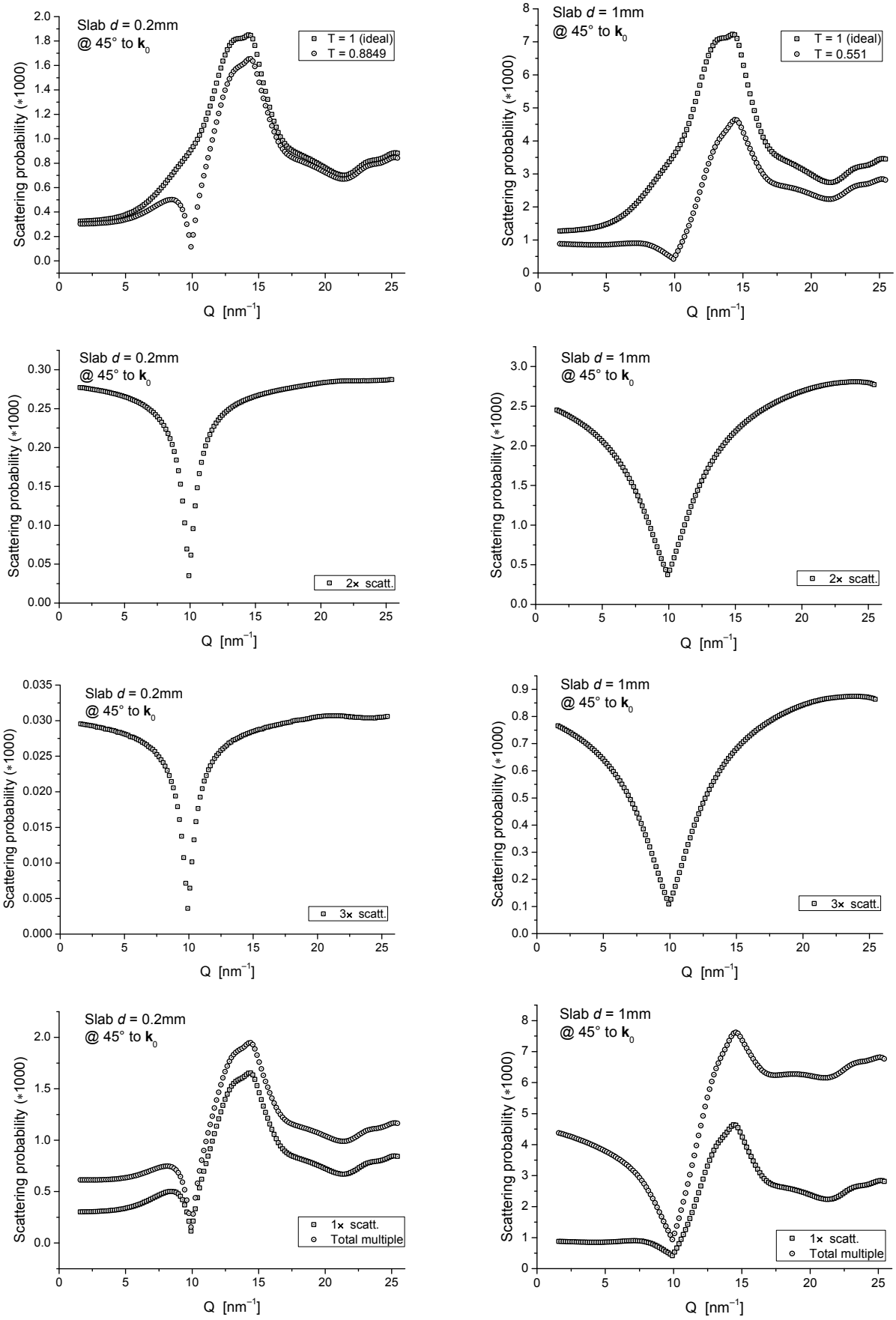

Fig. 3-5. Illustration of multiple scattering and self-extinction effects on coherent scattering from a flat sample of atactic polystyrene. Left column: thin sample, right column: thick sample. Unpublished results. More explanation in text.

4 Fundamentals of Small Angle Neutron Scattering

Small Angle Neutron Scattering is a routine neutron scattering technique, widely used to characterize large scale molecular systems in chemistry, polymer sciences and biology. This subject is covered in virtually all academic texts on neutron scattering [8], and in dedicated books, e.g. [42]. One of the most useful and friendly introductions is due to S. M. King [43]. Consequently, this short chapter is aimed at mere introducing the subject, and is left without details on model data analysis.

If the coherent cross section is given by:

$$\frac{d\sigma}{d\Omega} = b_{coh}^2 \left\langle \left| \int \exp\left(-i\mathbf{Q}\mathbf{r}\right) n\left(\mathbf{r}\right) d\mathbf{r} \right|^2 \right\rangle \tag{4.1}$$

then at very small *Q:*

- All nuclei within a given volume will scatter in phase (no significant changes to the phase factor among the neighbouring atoms)
- One can average the nuclear scattering potential (the scattering length) over length scales $\sim \frac{2\pi}{10Q}$. This average is called the scattering length density (sometimes SLD) and usually denoted $\rho\left(\mathbf{r}\right)$.

At very small *Q* the coherent scattering will then be probing spatial fluctuations of $\rho\left(\mathbf{r}\right)$. In the rest of this chapter the term *particle* will refer to a defined region in space with ρ different from the surrounding (e.g. molecular aggregates in solution). After transformation of (4.1) one obtains:

$$\frac{d\sigma}{d\Omega} = \left(\rho - \rho_0\right)^2 \left|F\left(\mathbf{Q}\right)\right|^2 N_P \int_{space} G_P\left(\mathbf{r}\right) e^{i\mathbf{Q}\cdot\mathbf{r}} d\mathbf{r} \tag{4.2}$$

where G is the particle-particle correlation function (the probability that there is a particle at **r** if there is one at the origin) and $\left|F\left(\mathbf{Q}\right)\right|^2$ is the particle form factor:

$$\left|F\left(\mathbf{Q}\right)\right|^2 = \left\langle \left| \int_{\text{particle}} e^{i\mathbf{Q}\cdot\mathbf{x}}\, d\mathbf{x} \right|^2 \right\rangle_{\text{orientation}} \tag{4.3}$$

The expression for the cross section is the same as that for nuclear scattering except for the addition of a form factor that appears because the scattering is no longer from point-like centres. Introducing the sample volume V, the particle volume V_P, and the number of particles we may write the expression for the scattering intensity (identical particles):

$$I(\mathbf{Q}) = \frac{N}{V}\left(\rho_p - \rho_0\right)^2 V_p^2 \left\langle \left| \frac{1}{V_p} \int_{\text{particle}} e^{i\mathbf{Q}\mathbf{r}} d\mathbf{r} \right|^2 \right\rangle \quad . \tag{4.4}$$

The expression $\frac{N}{V}\left(\rho_p - \rho_0\right)^2 V_p^2$ is called the *contrast factor*. Scattering at $Q = 0$ will then read:

$$I(0) = \frac{N}{V}\left(\rho_p - \rho_0\right)^2 V_p^2 \tag{4.5}$$

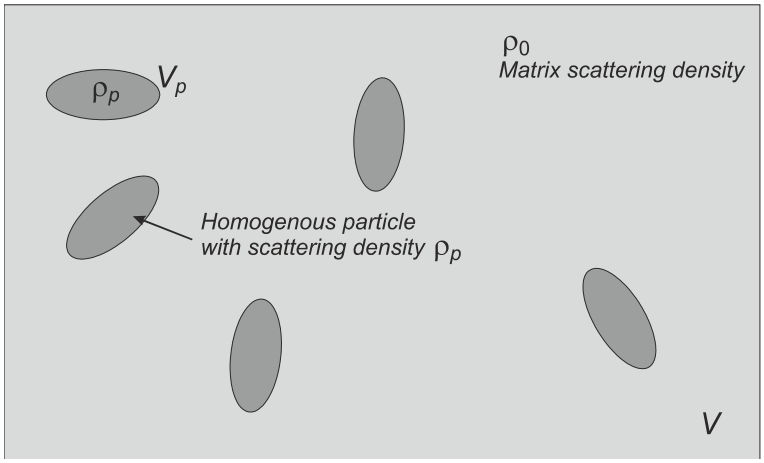

Fig. 4-1. The concept of contrast in SANS.

The particle form factor is determined by the particle shape. For a sphere of radius R, $F(Q)$ only depends on the magnitude of Q:

$$F_{sphere}(Q) = 3V_0\left[\frac{\sin QR - QR\cos QR}{(QR)^3}\right] \equiv \frac{3V_0}{QR} j_1(QR) \to V_0 \text{ at } Q = 0 \tag{4.6}$$

Form factors for other typical shapes such as cylinder, hollow cylinder, rod, disk, flat slab, etc. have been calculated analytically and are available from neutron scattering texts e.g. [43].

Eq. (4.2) can be once again rewritten in the following form, this time assuming the sample is isotropic [43]. Incoherent background is included explicitly. In most cases the latter can be eliminated by measuring a proper standard. More on this issue below.

$$\frac{\partial\sigma}{\partial\Omega}(Q) = N_p V_p^2 (\Delta\rho)^2 F(Q) S(Q) + B_{inc} \tag{4.7}$$

In the formulation of Eq. (4.7), the cross section is expressed in terms of the product of form factor $F(Q)$ and the structure factor $S(Q)$. The form factor is a function that describes how the scattering cross section is modulated by the interference effects of the radiation scattered on different parts of the same object. In particular, it depends on the shape of the object. Its general formulation is due to Van de Hulst [44].

The structure factor:

$$S(Q) = 1 + \frac{4\pi N_p}{QV} \int_0^\infty \left[g(r) - 1 \right] r \sin(Qr)\, dr \tag{4.8}$$

is a function that describes how the scattering cross section is modulated by the interference effects of the radiation scattered on **different objects.** In particular, it depends on a degree of local order in the sample. Hence SANS gives information on the relative position of scattering objects at least via the ***radial distribution function:***

$$G(r) = \frac{4\pi N_p r^2}{V} g(r) \tag{4.9}$$

Here $g(r)$ can be obtained by the Fourier transform of the structure factor $S(Q)$ (Eq. (4.8)), and N_p is the number density of scattering objects. Small angle neutron scattering is in many cases the art of isotopic substitution. Not only is it important to maximize the contrast factor in (4.4), but in multiphase systems that pose unnecessary difficulties through more than one particle type, through isotopic substitution one can make a part of the system invisible to SANS through equating its mean scattering length to that of the surrounding. The operation of choosing the best contrast for a given experiment is called the *contrast match.* Isotopic substitution is unique for neutron scattering, hence the power this technique as compared to SAXS, small angle X-Ray scattering.

SANS data are conventionally analysed and displayed by means of specific approximations (sometimes referred to as "laws"), depending on the sample measured, its solution concentration (if applicable), and the Q region. The most common are due to Guinier, Zimm, Porod, Kratky.

- **The Guinier approximation** consists in plotting $\ln\left[I(Q) \right]$ vs. Q^2 under the assumption that the scattering intensity depends upon the gyration radius via:

$$I(Q) = I_0 \exp\left(-\frac{Q^2 R_g^2}{3} \right), \tag{4.10}$$

where R_g is the radius of gyration, measuring the "effective size" of the scattering object. The Guinier approximation is valid for $QR_g < \sqrt{3}$. There exist shape-specific variants of Guinier plots, e.g. for elongated or flat (lamellae) objects.

- **The Porod,** or "log-log" **plot** involves plotting $\log\left[I(Q)\right]$ vs. $\log(Q)$ (base-10 logarithm) and yields information about the so-called "fractal dimension" of the scattering objects. It relies on this approximation valid for high-Q region of SANS:

$$I(Q) = \frac{A}{Q^n} + B \tag{4.11}$$

An estimate for the fractal dimension is obtained through $n = 6 - D$. Moreover, for polymer samples *n* is related to the excluded volume parameter ν via $n = 1/\nu$.

- **The Zimm plot** contains the graph of I^{-1} vs. Q^2 and originates from the field of light scattering, where it is widely used. Here the Q-dependence of the scattering intensity is assumed Lorentzian:

$$I(Q) = \frac{I_0}{1 + Q^2\xi^2} \tag{4.12}$$

with ξ being the correlation length. The linear I^{-1} vs. Q^2 plot will have $1/I_0$ for its intercept and ξ^2/I_0 for its slope. At low-Q region the Zimm plot provides another estimate for the radius of gyration: $\xi = R_g/\sqrt{3}$. So:

$$I(Q) = \frac{I_0}{1 + \frac{Q^2R_g^2}{3}} \approx I_0\left[1 - \frac{Q^2R_g^2}{3} + \cdots\right] \tag{4.13}$$

Inhomogeneous or chain-branched polymer samples render Zimm plots deviating from a straight line at low Q, and phase-separated samples yield negative intercepts.

The Zimm plot works also in high-Q region providing another estimate for the excluded volume.

- **The Kratky plot** $Q^2I(Q)$ vs. Q works in the high-Q region of SANS. In polymer physics, it provides a good measure of Gaussian nature of polymer coils. Assuming that the scattering law for a Gaussian coil varies like $I(Q) \sim 1/Q^2$ in the high-Q region, the Kratky plot for such a sample should tend to a plateau. Any deviation from this is a signature of non-Gaussian nature of the polymer coil.

Many properties of polymer systems are measured by small angle scattering of the material in solution, often extrapolating to zero concentrations (e.g. Zimm, Guinier approximations). However, some characteristic of bulk polymer samples, such as fluctuations of scattering length density resulting from aggregating interactions in solid polymer electrolytes can also be analysed using SANS [45], however with much effort: Bulk polymer samples are never quite as homogenous as e.g. polycrystalline metals. Often a density distribution occurs on a microscopic scale, giving rise to parasitic scattering on voids, which has to be accounted for separately.

Many polymers exhibit small angle scattering characteristic for self-similar or fractal systems (the corresponding form factors are known [43]). In order to fully explore such systems it is desirable to measure coherent scattering over a very large span of *Q*. This means combining data from various instruments. In view of what has been said on the separation of coherent and incoherent scattering, SANS instruments equipped with polarization analysis would be of use, especially those operating at higher *Q*. The need for such an option is illustrated in Fig. 4-2, presenting data taken for the same sample on D7, the diffuse scattering instrument with polarization analysis, and LOQ, the SANS instrument at ISIS, Rurherford Appleton Laboratory.

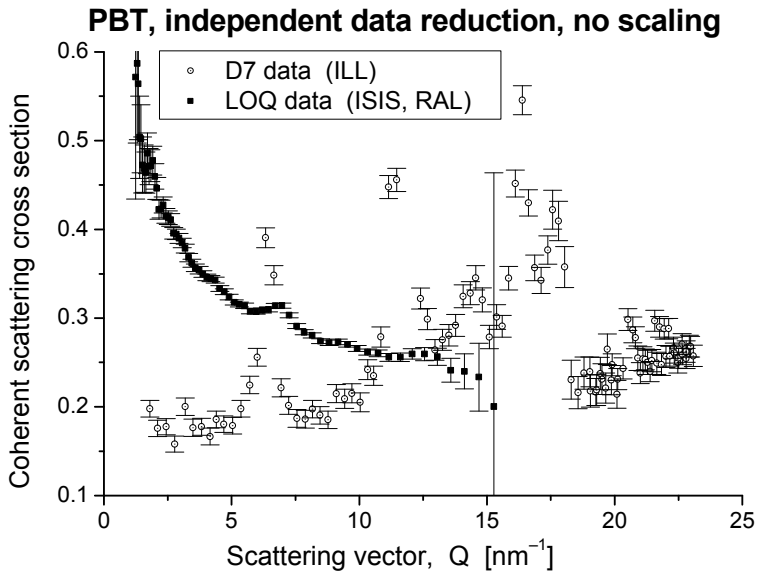

Fig. 4-2. Coherent neutron scattering from a sample of PBT, poly(butylene terephthalate) measured with polarized neutrons on D7, ILL and on LOQ instrument (high Q detector bank) at ISIS, RAL. Private communication from S.M.King.

At present, SANS instruments with polarization analysis are already available at some neutron sources (e.g. at Helmholtz-Zentrum, Berlin, or at LLB), or are planned (HFR2).

5 Short Range Order in Atactic Polystyrene

The term *short range order* usually refers to spatial correlations within the range of ca. 1 nm. Most often the use of this term implicitly suggests the lack of long range order, as otherwise one would speak of ordered phases or crystal structures and would use standard diffraction techniques in the study thereof. Polymers are often amorphous materials, although crystal or semicrystalline structures are not a rarity. Sometimes there are ordered regions coexisting with amorphous ones in chemically homogenous materials, or copolymers may exist, where one of the components forms an ordered phase. Such is the case of poly(urea urethane) elastomers discussed in Chapter 7, where hard segments tend to order and soft segments undergo order-disorder transitions, as revealed in DSC scans [18]. Complexation of poly(ethylene oxide) with a lithium salt (material of interest to the battery industry), PEO · $LiClO_4$ leads to the development of complex ordered structure, dependent on the salt concentration and on the molecular weight of PEO, as shown in Fig. 5-1.

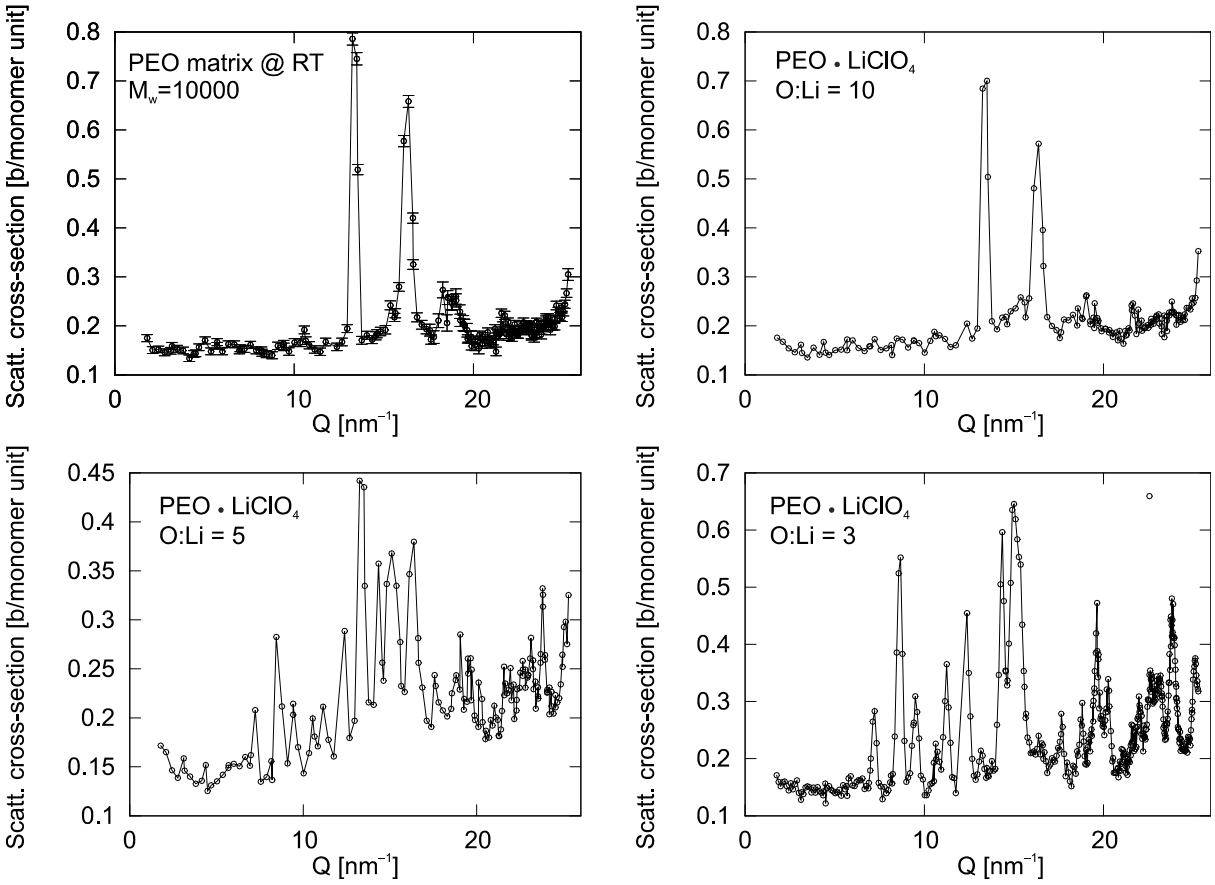

Fig. 5-1. Structure of PEO · $LiClO_4$ complexes dependent on the salt concentration. Measurement at D7, ILL at ambient temperature. Unpublished.

Polymer materials used throughout the rest of this report are amorphous in terms of crystallography, however showing various degree of short range order.

The idea that, despite the success of statistical description of random polymer structures, which we owe to pioneering works of Nobel Prize winner, Paul J. Flory (e.g. [46-48]), there nevertheless exists preferential arrangement of building units on a microscopic scale, slowly ploughed its way through the literature.

Structural properties of polystyrene (PS) have been extensively investigated for many years (see e.g. [29,49,50]. It looked as if a comprehensive study by Iradi et al. [49], combining neutron scattering and molecular simulation techniques, indeed *dotted the i's and crossed the t's.* However, there still seems to be a lot of work in front of the researchers, in particular on the contribution of inter- and intrachain correlations to the short range order. Indeed, some features of coherent neutron scattering spectra of atactic polystyrene, attributed to intermolecular correlations in the paper mentioned [49], can in fact be reproduced in a calculated coherent spectrum of a single PS random coil.

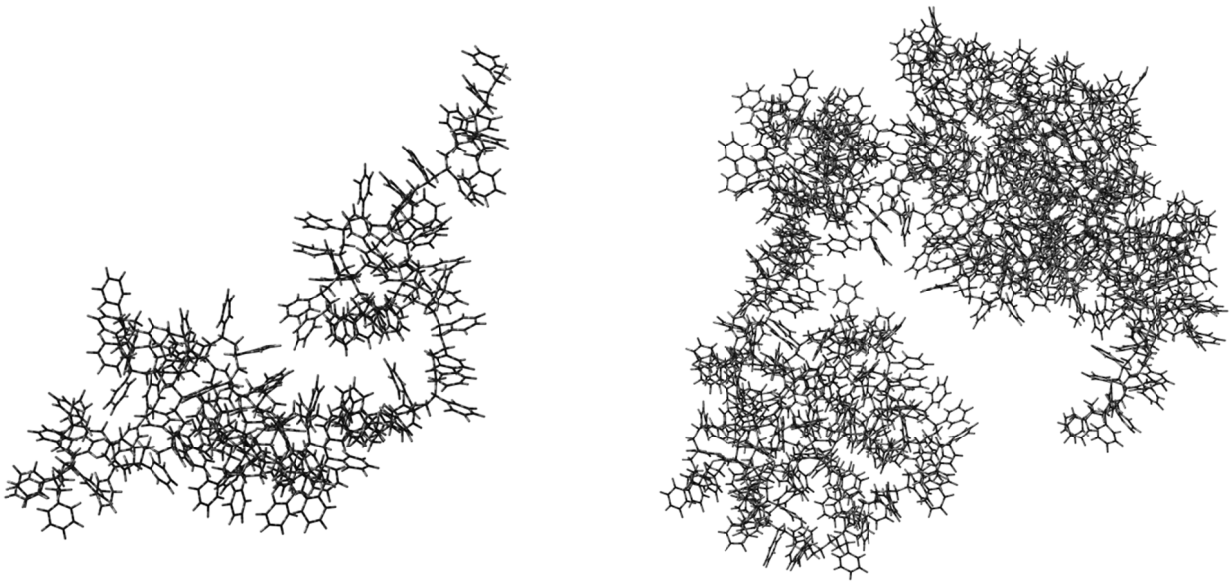

Random chains of atactic polystyrene composed of 100 and 400 building units were computer-generated by a head-to-tail random addition of consecutive segments. So obtained structures were subjected to configurational energy minimization, and then thermal vibrations at arbitrary

temperature of 350K were allowed for the time long enough to reach equilibrium. The resulting structures are shown in Fig. 5-2. Coherent neutron scattering spectra were then calculated for such objects, from the first principles.

Unlike proposed in [37,51], the polymer coil was not treated as composed of monomer building units treated as scattering objects of averaged properties, because such an approach, although simplifies the calculations, effectively eliminates a significant number of atom-atom correlations from being considered.

In studying neutron scattering from polymer chains, most of the theory presented in Veinshtein's book on X-Ray diffraction from chain molecules [52] can be utilized, especially in case of partially ordered chains of isotactic or syndiotactic PS, as proposed in [37]. Here, for a Gaussian polymer chain, being an ensemble of N nuclei a coordinates $\mathbf{r}_i$,it is enough to calculate $I_{coh}(Q)$ from Eq. (2.14), assuming various atomic species:

$$\left[\frac{d\sigma(\theta)}{d\Omega}\right]_{coh} = I_{coh}(Q) = \frac{1}{N}\sum_{i,j}^{N}\left\langle b_i b_j \exp\left(i\mathbf{Q}\mathbf{r}_{ij}\right)\right\rangle, \tag{5.1}$$

where angular braces indicate spherical averaging over all possible spatial orientations of the polymer coil. It can be shown [51], that Eq. (5.1) then simplifies to:

$$I_{coh}(Q) = \frac{1}{N}\sum_{i,j}^{N}\langle b_i\rangle\langle b_j\rangle\frac{\sin Qr_{ij}}{Qr_{ij}} \tag{5.2}$$

Averages $\langle b_i\rangle$, $\langle b_j\rangle$ include isotopic diversity. Fig. 5-3 displays the result in its left panel, and for comparison it presents coherent scattering from a sample of atactic PS measured on the D7 instrument at the ILL (right panel).

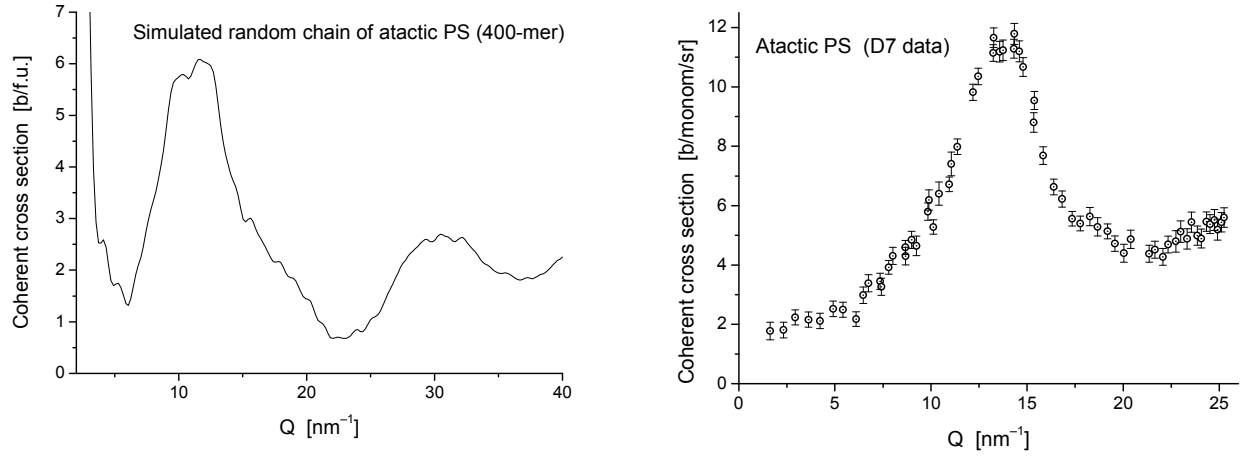

Fig. 5-3. Left graph: Calculated coherent neutron scattering from a computer-generated 400-mer of atactic PS. Right graph: Coherent scattering from atactic PS. D7 data.

Excess coherent intensity at low Q in Fig. 5-3 can be explained by the small size of the "sample" and it being isolated, i.e. by the lack of interchain correlations. This region has therefore to be considered unphysical. The main feature (above 10 nm^{-1}), however, resembles real data surprisingly well. The only difference can be found in its position on the Q-axis. It is very likely, that a computer-generated PS chain is a more sparse structure than a real PS sample, which could lead to larger correlation distances and, consequently, to coherent scattering maxima at lower Q values. Density calculated for a chain depicted in Fig. 5-2 is unreliable due to difficulties in estimation of its true volume, and therefore cannot be compared to the value known for atactic polystyrene.

A conclusion can therefore be drawn from the results of [49] and from the above example that the central twin peak in the coherent scattering from atactic PS cannot be uniquely attributed to intra- or interchain correlations. Rather, it results from the proximity of the polymer building units and their mutual preferred arrangement, no matter to which chain they belong. This, in turn, indicates that interactions leading to the onset of short-range order may involve small polymer subunits, or maybe chemical sub-structures (groups).

Another reason for presenting Fig. 5-2 is the illustration that real polymer networks may display features of limited self-similarity. This is why the description of e.g. small angle scattering data from "swollen coils" of certain polymers involves the use of formulae derived for fractal objects.

6 Miscibility of Polymer Blends and the Short Range Order

6.1 Introduction

Blending of polymers is an important means, widely used by industry, to obtain a product of desired properties, better than constituent polymers. Improved physical and chemical properties, such as clarity, solvent resistance, mechanical endurance or capability of shock absorbing, can be obtained without having to synthesise new materials. The successful mixing of several polymers can be described by their miscibility, and that in turn can be determined by various experimental techniques. Traditionally, miscibility is a macroscopic quantity calculated from thermodynamical theories [53] and measured by several techniques such as differential scanning calorimetry (DSC). It is however a question of scale: the miscibility is as good as the technique used to determine it. There is no guarantee that the optically miscible blend remains thoroughly mixed on the molecular level. In order to approach the miscibility from the microscopic point of view, techniques such as small angle neutron scattering (SANS) are widely applied to the studies of blends [53]. SANS accesses large-scale structures and allows one to determine the extent of phase-separation, which is then linked to the miscibility [54]. In order to descend to the molecular level, wide angle (or diffuse) scattering techniques, both X-ray and neutrons, can be used to probe the structure [53,55]. The known problems with the interpretation of "amorphous halo" (X-ray)and dominant incoherent neutron scattering from hydrogen-rich samples mean that these techniques were used relatively little to date, especially for the studies of such complex materials as blends. However, the application of the wide angle scattering of polarised neutrons with spin polarisation analysis to ionomers [56] and their blends [57-59] offers a way to change this.

6.2 Destruction of short range order in PC-SPS blends

In general, polymers do not mix well and they often require the including of ionic groups (see e.g. [60]) or compatibilizing agents in order to make a good mixture. A large number of factors influence the miscibility of polymer blends, and the tendency of the components to assume

short-range preferential arrangement (short range order) counts among them. In order to check the behaviour of short range order, a partially miscible system of bisphenol-A-polycarbonate and sulphonated polystyrene ionomers was studied by means of diffuse scattering of polarised neutrons [57].

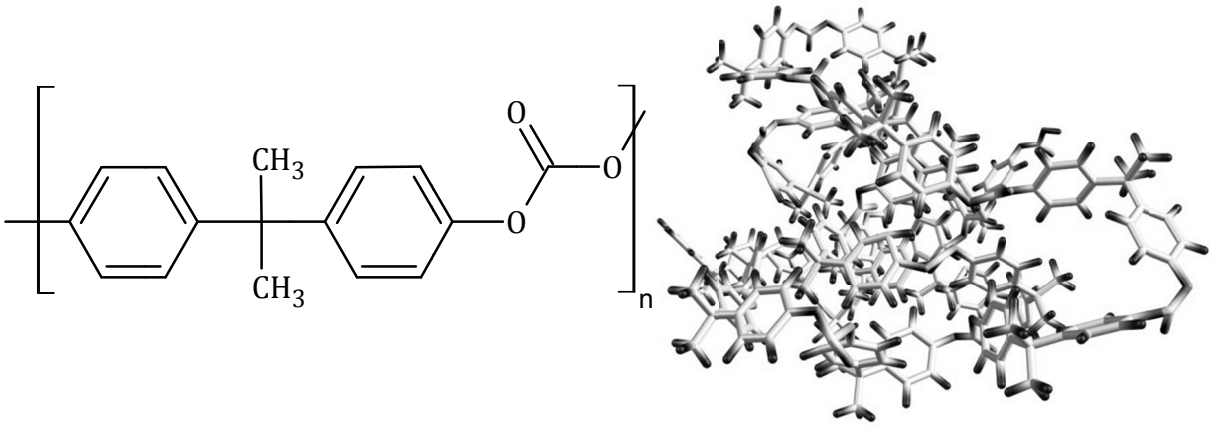

This system was chosen because polycarbonate (PC) is very often blended with other polymers, and its blends with sulphonated PS (SPS) (Fig. 6-2) had been previously studied (see e.g. [61,62]). It was shown that strong repulsive interactions between the ionic and non-ionic groups within the ionomer facilitate mixing and are responsible for the phase behaviour of the blend (op. cit.). Sulphonated polystyrene used in this study was neutralized with monovalent ions of lithium and sodium (for reference). The samples were kindly provided by prof. Robert Weiss (Univ. of Connecticut). The degree (extent) of short range order was assessed by measuring diffuse coherent neutron scattering (ILL, instrument D7, scattering of polarized neutrons with polarization analysis).

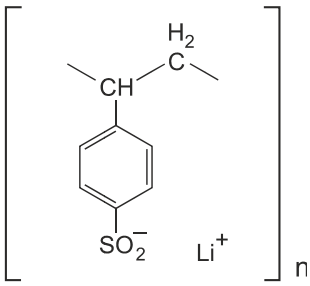

ıilding

Figure 6-3 presents coherent scattering from the component polymers (polycarbonate and lithium-sulphonated polystyrene). A coherent spectrum from the atactic PS standard is also presented for comparison.

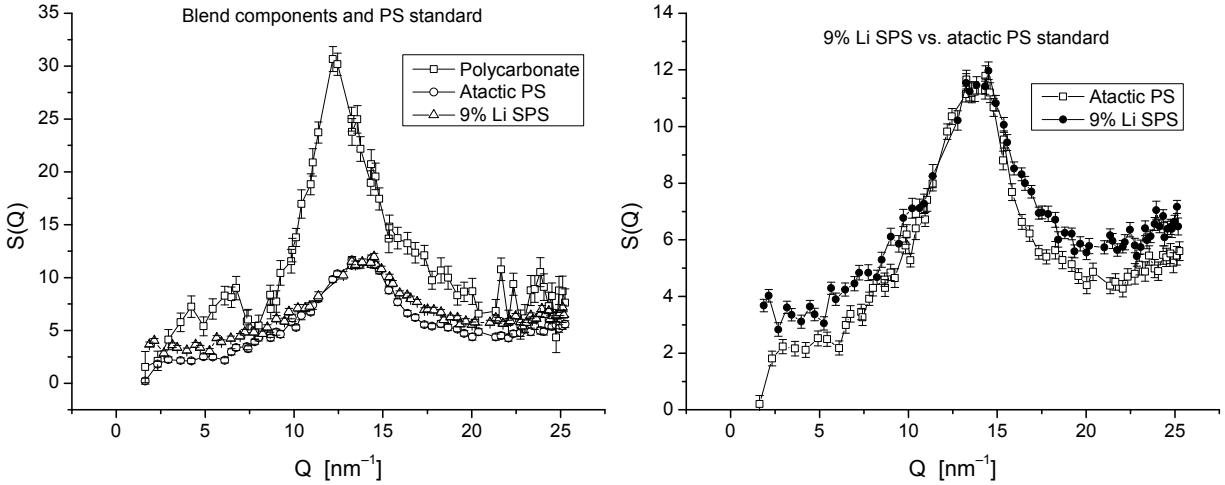

Fig. 6-3. Coherent diffuse neutron scattering from the blend components compared with atactic polystyrene standard.

The first peak in the PC spectrum around Q = 6 nm^{-1} (Fig. 6-3, left panel) is attributed to the correlations between the carbonate groups, with added influence of the isopropylidene groups [63]. Correlation between adjacent chains produce the tall peak around Q = 16 nm^{-1} [63,64]. The peak position measures the mean spacing between chains $D = \frac{2\pi}{Q}$, while its width provides an estimate to the correlation length $\xi = \frac{4\pi}{\Delta Q}$.

The results for pure PC are presented in Table 6-1, along with those of other authors:

Table 6-1. Short range order parameters of polycarbonate (cf. [57]**)**

	This work	Lamers et al. [64]	Eilhard et al. [63] (measured)	Eilhard et al. [63] (simulated)
Spacing, D [nm]	0.5 (±0.01)	0.495	0.493	0.519
Corr. l., ξ [nm]	3.53 (±0.01)	2.8	2.76	2.243

The obtained results are in excellent agreement with literature data, taking into account the possible influence of sample preparation details, which could have differed.

Fig. 6-4 illustrates the dependence of short-range order in three blends of polycarbonate with pure and lithium-sulphonated polystyrene upon the blend composition. At room temperature all these blends are immiscible (PS/PC is immiscible at all temperatures). The addition of immiscible PS or SPS results in the disappearance of the small peak around Q = 16 nm^{-1} with hardly any effect upon the main peak, other than its intensity connected with the blend composition.

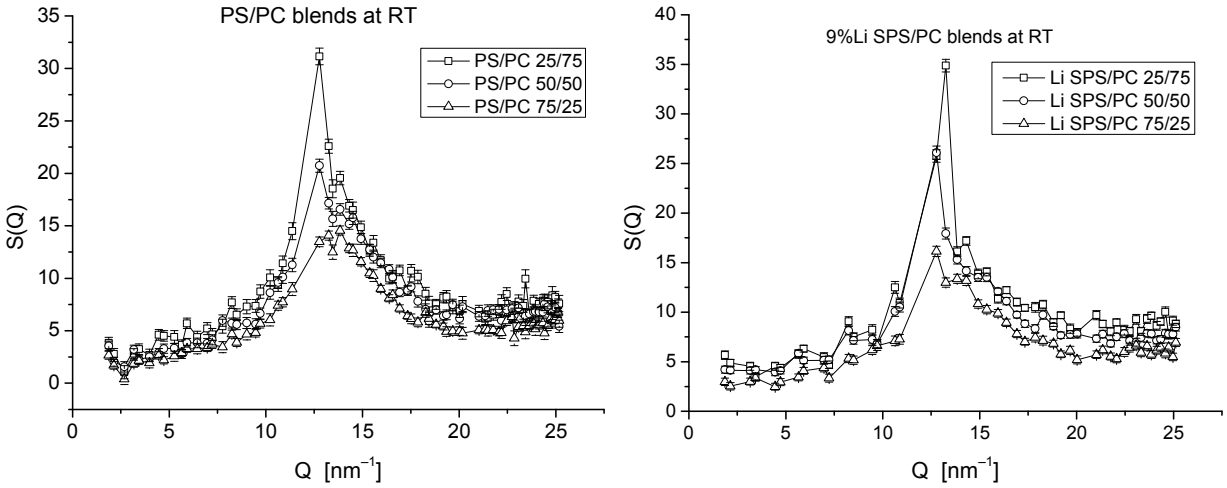

Fig. 6-4. Coherent neutron scattering from three PS/PC and three Li SPS/PC blends as obtained by diffuse scattering of polarized neutrons with polarization analysis. (cf. [57]**)**

9%Li SPS /PC blends exhibit upper critical solution temperature (UCST) properties (see Appendix to this chapter) with typical critical temperatures ranging from 170°C to 260°C, depending on the sulphonation level of the ionomer and on the molecular weight of the polymers. Critical temperatures for the samples used here were estimated to be ca. 443K [61]. Miscibility of polystyrene ionomers – polycarbonate blends depends not only upon the properties of polymers in question (including degree of sulphonation): an important role is also played by the counterion, even same valency [61].

Diffuse (wide angle) scattering (WANS) of polarised neutrons was measured for three compositions of 9%Li SPS/PC (25/75%, 50/50%, 75/25%) at room temperature (RT) and well above the critical point. For reference, the same compositions at same temperatures were measured for immiscible 5.1%Na SPS/PC blends. The resulting WANS spectra are shown in figures 6-5 and 6-6. The "destructive" effect of mixing upon the short range order is well seen.

Comparison with the immiscible 5.1%Na SPS/PC system provides an evidence that the effect is indeed due to the mixing and not any other factor.

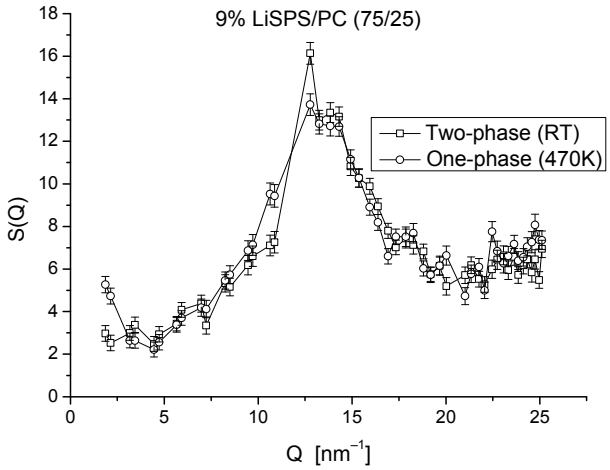

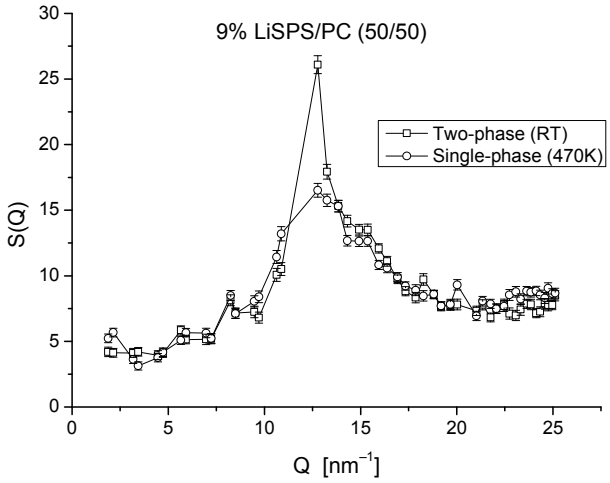

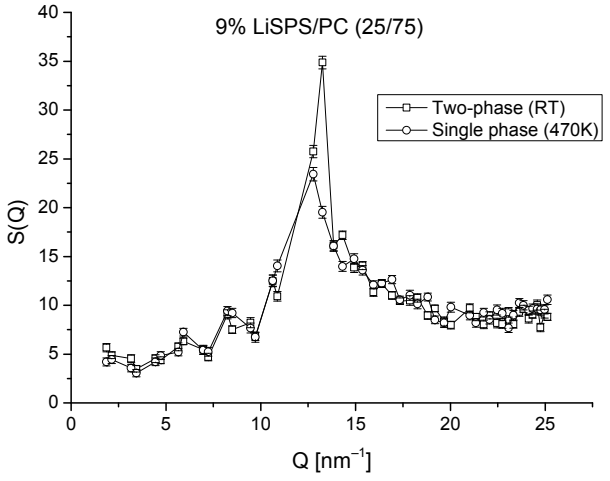

Fig. 6-5. Coherent neutron scattering spectra for 9%Li SPS/PC blends at room temperature and above the critical point. (cf. [57]**)**

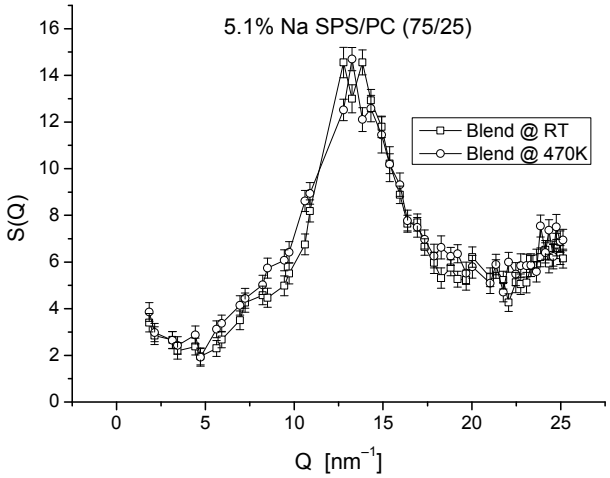

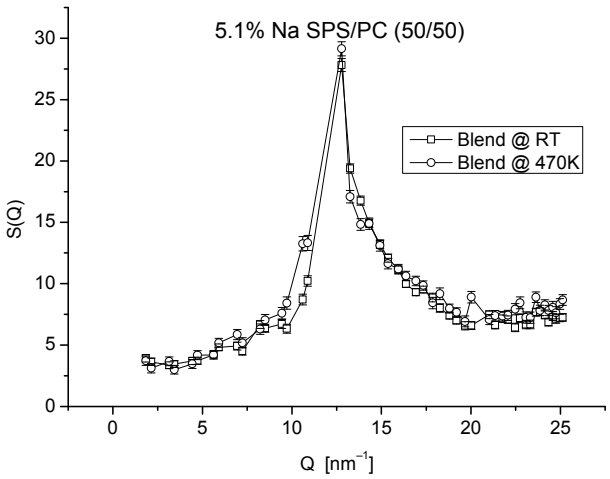

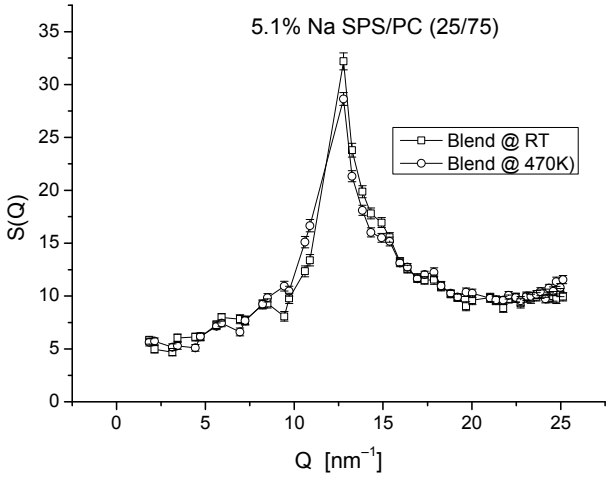

Fig. 6-6. Coherent neutron scattering spectra for 5.1Na SPS/PC blends at room temperature and at 470K. (cf. [57]**, partially unpublished)**

From the WANS spectra shown in Fig. 6-4 one can deduce the following decrease in the mean correlation length of neighbouring PC chains:

Table 6-2. Interchain correlation lengths in 9% Li SPS/PC blends . (cf. [57]**)**

composition	75/25	50/50	25/75
ξ, Phase-separated region [nm]	2.08	4.96	5.51
ξ, Single phase region [nm]	1.69	1.15	0.76

To the author's knowledge, this was the first approach to the study of correlation of polymer blend miscibility with the degree of short range order by means of diffuse (wide angle) neutron scattering of polarized neutrons with polarization an analysis. A carefully planned experiment of this type may prove helpful in solving puzzles in this field of materials science.

6.3 SANS study of SPBT-PC$_d$ blends

Polymer blends are routinely studied by small angle neutron scattering. With this method one can assess whether the blend under consideration is miscible, partly miscible or immiscible. In case of more complex compositions, the contrast variation through isotopic substitution helps one to extract the needed information. In phase-separated systems one can study spatial properties of the volume occupied by a given phase. Such a study was undertaken for a relatively little known blend of sulphonated poly(butylene terephthalate) (SPBT) with amorphous polycarbonate [54]. Poly(butylene terephthalate) (PBT) is a technologically important thermplastic, yet in order to improve its properties, it is blended with other components. However, its semicrystalline structure makes it opaque and results in poor mixing. Random sulphonation of PBT (a random copolymer of PBT and sulphonated PBT) counteracts crystallization and makes mixing easier.

The influence of different levels of sulphonation upon the properties of poly(butylene terephthalate) had been previously studied by wide angle X-ray scattering (WAXS), polarised light microscopy and small angle light scattering (SALS). The type of spherulitic structure found

in these polyesters depends upon the sulphonation level, as does the degree of crystallinity; the latter decreases with ionic content while the spherulite radius remains relatively constant.

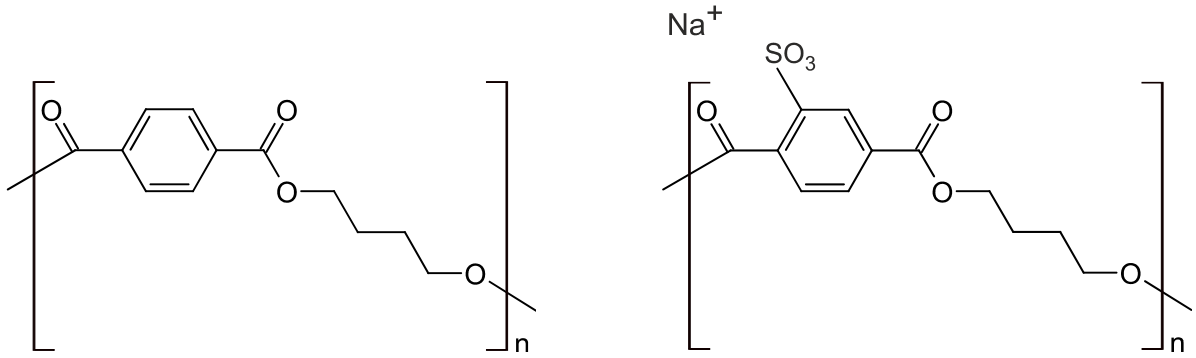

Fig. 6-7. Chemical structures of PBT (left) and SPBT (right).

Blends used for the SANS experiment (ISIS, Rutherford Appleton Laboratory, instrument: LOQ [65,66]) contained fully deuterated polycarbonate (PC_d).

Table 6-3. Samples used in the SANS study of SPBT/PCd blends. (cf. [54]**)**

Sample	Blend composition % w/w
PC_d	100
PBT	100
3.5mol % SPBT	
7.9mol% SPBT	
11.1mol% SPBT	
PBT/ PC_d	75/25
PBT/ PC_d	50/50
3.5 mol % SPBT/ PC_d	75/25
3.5 mol % SPBT/ PC_d	50/50
7.9 mol % SPBT/ PC_d	75/25
7.9 mol % SPBT/ PC_d	50/50
11.1 mol % SPBT/ PC_d	90/10
11.1 mol % SPBT/ PC_d	75/25

From the small angle neutron scattering point of view, a phase-separated mixture is composed of scattering objects of unidentified size and shape. If so, then the SANS data can be described using the Debye–Bueche expression [67]:

$$I(Q) = \frac{A}{\left(1 + Q^2 a_c^{\,2}\right)^2} \tag{6.1}$$

where a_c is the corresponding correlation length of the blend, which may be interpreted as the size of the density fluctuations, and the parameter A – the zero-angle scattering – is related to the thermodynamic properties of the blend. Sample fits to this mode in linearizer representations are shown in Fig. 6-8.

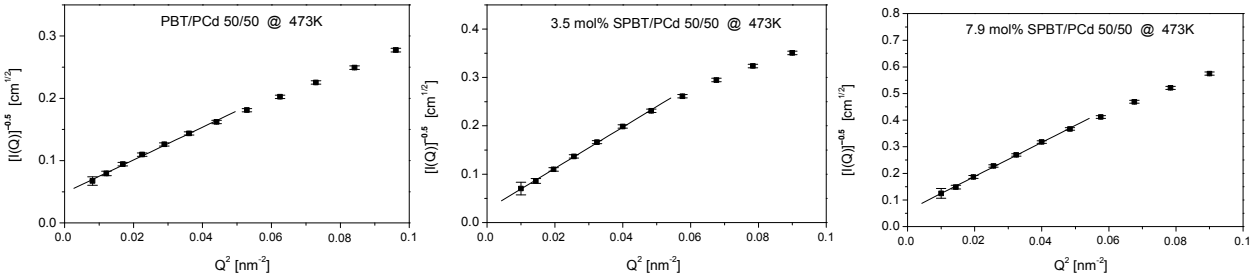

Fig. 6-8. Debye-Bueche plots of SANS data taken at 473K for 50/50 blends of: PBT/PCd (left), 3.5 mol% SPBT/PCd (middle) and 7.9 mol% SPBT/PCd (right) (cf. [54] **)**

The a_c parameter in Eq. (6.1) is also a measure of the average size of heterogeneity [68]. Knowing the correlation length, the average transversal lengths through the two phases can be calculated. Hence $\overline{L_1} = a_c/\phi_1$ for the crystalline phase and $\overline{L_2} = a_c/\phi_2$ for the amorphous phase, where ϕ is the composition (cf. discussion and references within [54]). The degree of miscibility between the phases can be quantified through the second derivative of the Gibbs free energy of mixing, $\frac{\partial^2 G_m}{\partial \varphi^2}$; ($\varphi$ is the volume fraction of one phase) and the interaction parameter, $\chi_{1,2}$, calculated from [69]:

$$\frac{V}{I(0)} = \frac{1}{\nu_0\left(\frac{b_1 - \beta\, b_2}{V_1}\right)^2}\left[\frac{1}{\phi_1 N_1} + \frac{1}{\phi_2 N_2} - 2\chi_{1,2}\right] = \frac{1}{\nu_0\left(\frac{b_1 - \beta\, b_2}{V_1}\right)^2}\frac{\left(\frac{\partial^2 G}{\partial \varphi^2}\right)}{k_B T} \tag{6.2}$$

From the Debye-Bueche model, when applicable, the following results were obtained:

Table 6-4. Parameters obtained from the Debye-Bueche model fits to the data (when applicable), [54].

Sample	Blend composition	Temperature	A	a_c	L_1	L_2	$\frac{\partial^2 \Delta G_{mix}}{\partial \phi^2}$	$\chi_{1,2}$
	% w/w	K	cm^{-1}	nm	nm	nm	$/10^{-3}$	$/10^{-3}$
PBT/PC_d	50/50	438	332	7.1 ± 0.1	12.4	16.5	1.19	12.32
PBT/PC_d	50/50	473	290	6.8 ± 0.1	11.9	15.8	1.37	12.24
PBT/PC_d	50/50	488	199	6.3 ± 0.1	11.0	14.6	1.98	11.93
3.5 mol% SPBT/PC_d	75/25	488	5275	18.0 ± 0.3	59.4	25.8	0.08	20.22

The Debye-Bueche approach worked well at small momentum transfers. For all but one PBT/PC_d blends this model proved satisfactory at all temperatures studied. However, for most SPBT/PC_d compositions examined, it failed to reproduce experimental data, and a two-correlation-lengths model [68,70] had to be applied:

$$I(Q) = \frac{A_1}{\left(1 + Q^2 a_1^{\,2}\right)^2} + A_2 \exp\left(-\frac{Q^2 a_2^{\,2}}{4}\right) \tag{6.3}$$

This situation is illustrated in Fig. 6-9, and it appears typical of blends that are only partially

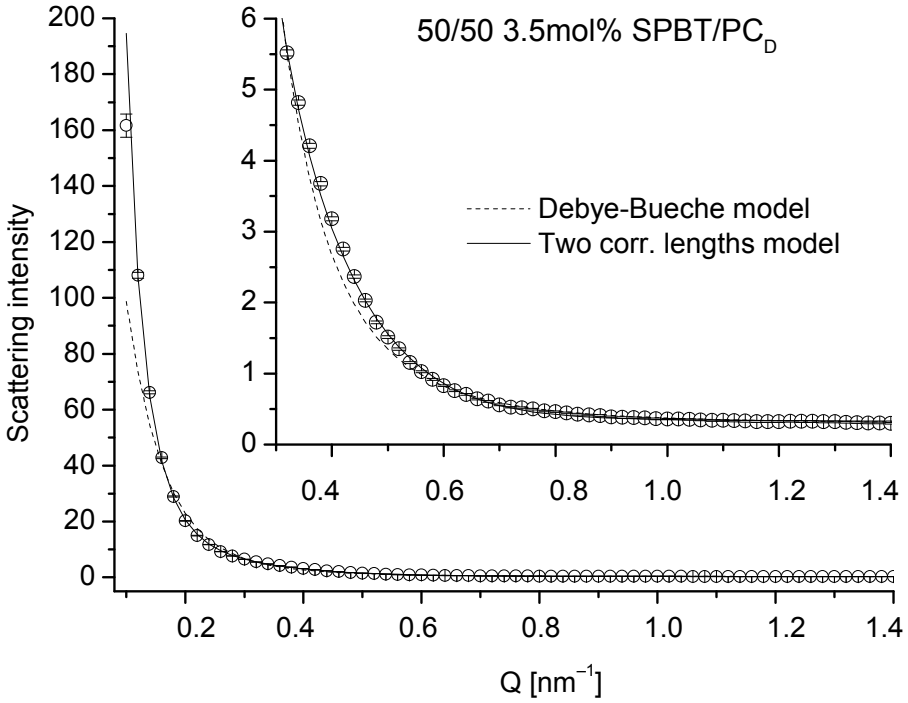

Fig. 6-9. SANS pattern from the 50/50 blend of 3.5mol% SPBT/PCd at 473K. The inset figure shows a close-up of the I(Q) plot for small intensities ([54]**)**

miscible, but not completely phase separated [71]. A single correlation length cannot describe scattering from such blends.

The derivation of Eq. (6.3) is straightforward if we notice that the Debye-Bueche model Eq. (6.1) is the Fourier transform of a simple correlation function assumed for the system: [70]

$$\gamma(r) = \exp\left(\frac{-r}{a_c}\right) \tag{6.4}$$

In case of systems that cannot be described by a single correlation function of type (6.4), e.g. in semicrystalline blends, the following two-term correlation function was developed [72]:

$$\gamma(r) = f\exp\left(\frac{-r}{a_1}\right) + (1-f)\exp\left(\frac{-r^2}{a_2^2}\right), \tag{6.5}$$

leading to Eq. (6.3) through the Fourier transform, with the relative contribution f connected with a_1, a_2, A_1 and A_2 via:

$$f = \frac{A_1}{A_1 + 8\sqrt{\pi}\left(\frac{a_1}{a_2}\right)^3 A_2}. \tag{6.6}$$

In the two-correlation-lengths model (6.3), a_1 accounts for the short range, and a_2 for long range correlation lengths. Then, the A_1 and A_2 coefficients may be related to the relative contributions of amorphous and crystalline behaviour. Fits of the quality shown in Fig. 6-9 lead to the values for parameters of interest listed in table 6-5.

Extensive discussion of the measurements on this particular system, data analysis and the meaning of the derived parameters is given in [54]. Small angle neutron scattering provided data sufficient to carry out a quantitative description of the miscibility of the SPBT/PC_d blends, being controlled by temperature, composition and particularly sulphonation levels. The values of L_1 (crystalline phase size) and L_2 (amorphous phase size) showed that the proportion of crystalline phase in the PBT/PC_d blend is consistent with the results obtained from DSC [73].

These materials still remain new and relatively little information is available among published papers. A somewhat corresponding study by small angle X-ray scattering was published in 2005 [74]. This does not mean that leading industrial laboratories are short of information on miscibility of technologically important blends. High quality samples used in this study were kindly provided by Exxon Research & Engineering.

Table 6-5. Parameters obtained from the two-correlation length model fits to the data [54].

Sample	Blend Comp.	Temp.	A_1	A_2	a_1	a_2	$\frac{\partial^2 \Delta G_{mix}}{\partial \phi^2}$	$\chi_{1,2}$
	% w/w	K	cm^{-1}	cm^{-1}	nm	nm	$/10^{-3}$	$/10^{-3}$
PBT/PC_d	75/25	433	481	0.15	1.1±3.6	7.3±0.14	0.83	20.11
3.5mol% SPBT/PC_d	75/25	438	16869	8.72	6.3±0.1	23.7±2.2	0.02	20.25
3.5mol% SPBT/PC_d	75/25	473	21143	11.58	6.5±0.1	25.6±2.9	0.02	20.25
3.5mol% SPBT/PC_d	50/50	438	4292	0.53	4.5±0.1	19.6±0.3	0.09	13.95
3.5mol% SPBT/PC_d	50/50	473	5870	6.11	5.7±0.1	21.3±1.8	0.07	13.97
3.5mol% SPBT/PC_d	50/50	488	29092	9.27	5.6±0.1	34.4±14.	0.01	13.99
7.9mol% SPBT/PC_d	75/25	303	498	0.15	3.6±0.2	138.±0.2	0.82	19.56
7.9mol% SPBT/PC_d	75/25	433	5384	1.66	5.1±0.1	22.7±1.5	0.08	19.93
7.9mol% SPBT/PC_d	75/25	488	481	0.99	5.1±0.1	13.7±0.3	0.85	19.54
7.9mol% SPBT/PC_d	50/50	438	497	0.31	3.9±0.1	14.1±0.1	0.83	12.34
7.9mol% SPBT/PC_d	50/50	473	265	0.58	4.7±0.1	11.2±0.2	1.55	11.97
7.9mol% SPBT/PC_d	50/50	488	322	1.34	5.1±0.1	12.2±0.2	1.27	12.11
11.1mol% SPBT/PC_d	90/10	30	476	1.31	5.8±0.1	13.0±0.4	0.88	44.25
11.1mol% SPBT/PC_d	90/10	433	618	0.94	4.8±0.2	19.2±0.8	0.68	44.35
11.1mol% SPBT/PC_d	75/25	433	2220	0.75	5.3±0.15	14.5±0.4	0.19	19.66

6.4 The influence of counterion valency upon the short range order in ionomers

The success of the Debye-Bueche and two-correlation-lengths models in the study of miscibility of PBT/PC and SPBT/PC blends was partly due to the semicrystallinity of PBT and its

subsequent destruction by sulphonation, i.e. to a well-defined and strong mechanism preventing the creation of a homogenous mixture down to molecular level. It is not uncommon, however, that neither of the two correlation functions: Eqns. (6.4) or (6.5) satisfactorily describes the short range order in a phase-separated blend. In order to see this, we will now return to the systems discussed at the beginning of this chapter, i.e. to SPS/PC ionomer blends. Having established that a miscible blend exhibits much less short-range (local) order than do the components and an immiscible blend, we will now turn to small angle region of scattering [75].

As previously, the experiment was performed at ISIS Spallation Neutron Source, Rutherford Appleton Laboratory, instrument: LOQ [65,66]. Debye-Bueche plots of the measured data are presented in Fig. 6-10. It is evident that this approximation does not hold, especially at ambient temperature – top-left graph. The plots are nowhere linear. At 453K (180°C), the sample may be a combination of miscible and phase-separated regions due to possible peritransition effects. The

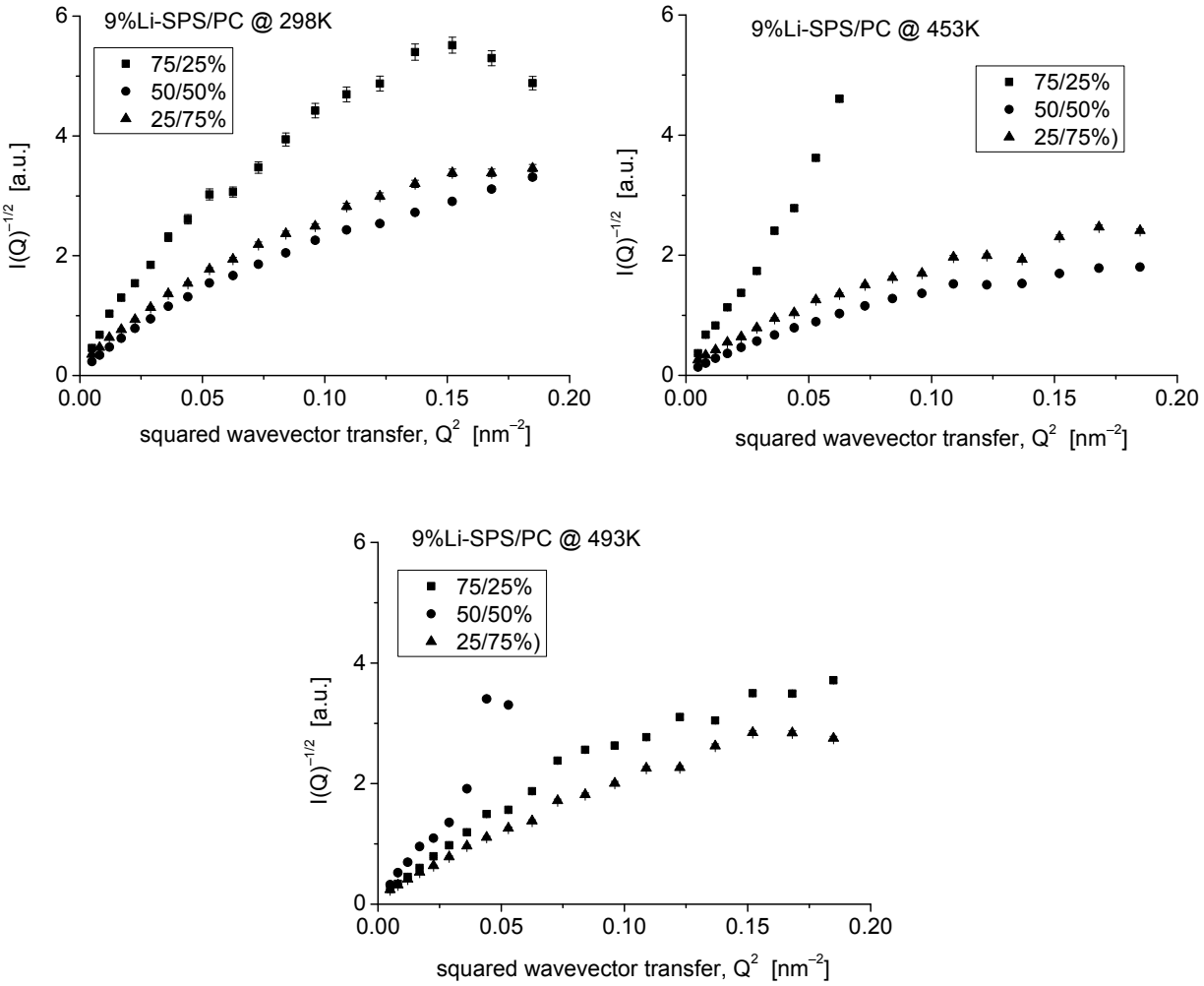

Fig. 6-10. SANS spectra of 9%Li-SPS/PC blends in the Debye– Bueche representation (cf. [75]**).**

situation at 493K (220°C) should not be surprising perhaps, as at this temperature the blend had been characterized as miscible and no phase separation was expected. However, data for the 25/75% composition look almost unchanged, and the 75/25% blend points reproduce the main course of 25/75%.

And what if the problem is caused by the ionomer itself rather than the interactions within the mixture? Analysing a Debye-Bueche plot of the pure SPS may be a strange idea, since this is to be expected a single-phase system. However, the graphs look linear, as if they represented a phase-separated system. This is illustrated in Fig. 6-11.

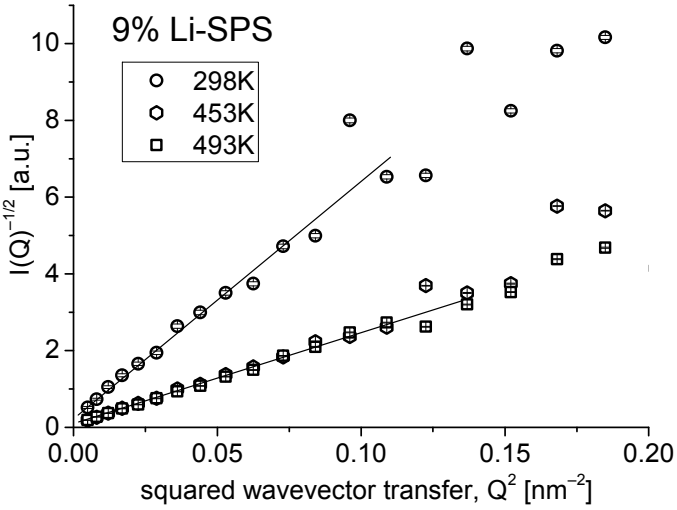

Fig. 6-11. Debye– Bueche representation of the SANS data for 9%Li-SPS (cf. [75]**).**

It is now evident that there are interactions within the ionomer such that they result in fluctuations of microvolume-averaged scattering length, similar to that seen in a phase-separated system. Properties of a random ionomer may depend not only upon the attached ionic group but also on the neutralizing counterion. This seems to be the case in sulphonated polystyrene. Aggregating interactions, if any, could show as additional short-range order in the coherent WANS spectra of the ionomer.

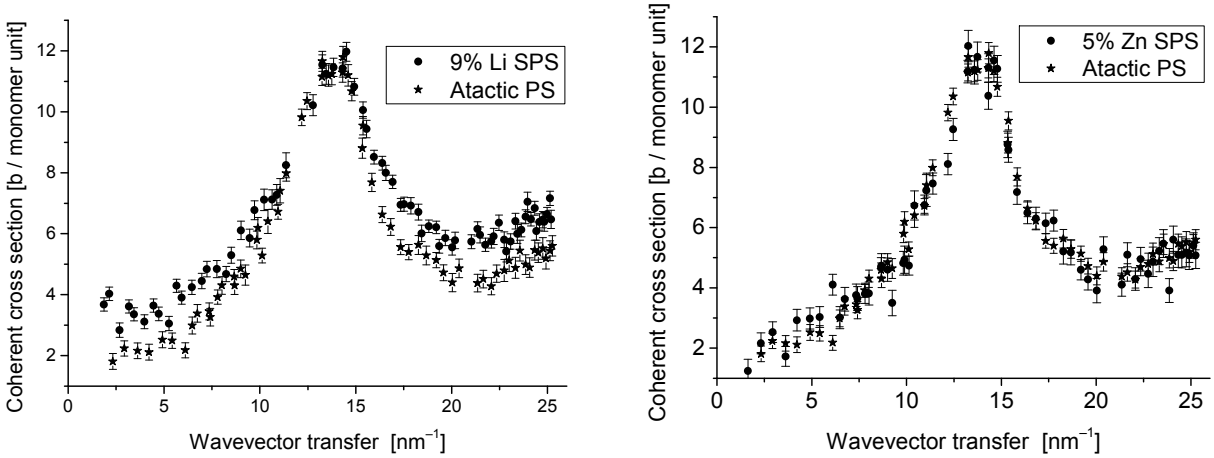

Fig. 6-12. Coherent wide angle neutron scattering spectra of 9% Li-SPS (left) and 5% Zn-SPS (right) compared with those of atactic polystyrene (cf. [75]**).**

Such additional coherent intensity is indeed seen on either side of the main WANS peak. Left graph of Fig. 6-12 compares WANS spectrum of 9% Li SPS with that of atactic PS. A similar comparison with zinc-sulphonated PS shows no such effect. A behaviour similar to that in lithium-sulphonated PS can be found also in 8.45% H SPS (Fig. 6-13). This may suggest that what matters is the valency of the counterion. The presence of ionic groups and counterions may lead to a number of interactions, depending on the sulphonation level and the counterion valency. Zhou et al. [76] report on this while studying the phase behaviour of sulphonated polystyrene systems. During the investigation of properties of random poly(lactic acid)-based ionomers Ro et al. [77] indicated the role of metallic counterion valency. Moreover, they found that the solubility of carboxylic acid-functionalized copolymer (COPOLYSA) increased as the valency of the cation increased, which they consider counterintuitive since higher-valency ions should form stronger ionic pairs. Complexation of acid groups in SPS is a known cause for poor miscibility of highly sulphonated polymer in blends.

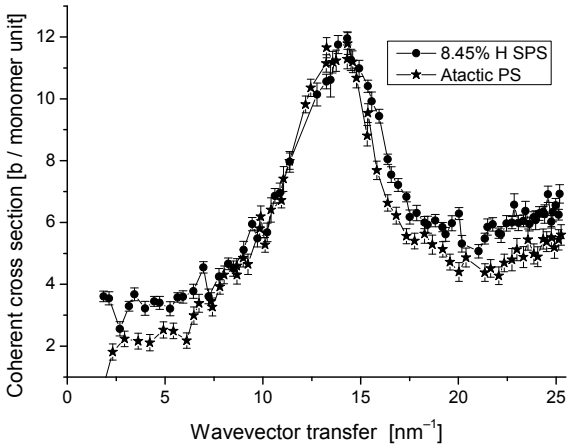

Fig. 6-13. Coherent wide angle neutron scattering spectra of 8.45% Li-SPS compared with that of atactic polystyrene. Unpublished data.

In search for the possible source of aggregating interactions in SPS a plausible hypothesis was put forward that such additional correlations may be caused by the presence of monovalent counterions: then the sulphonic groups are likely to enter into so-called π-complexes with π-electrons of the phenyl rings of polystyrene [78]. Another feasible mechanism involves interactions within closely positioned sulphonic groups. Acceptor-donor-type interactions may lead to the onset of "intermediate" chemical structures, as shown in Fig. 6-14 (top-right inset) [78]. These speculations are certainly inspiring and further research would shed more light on the interesting matter.

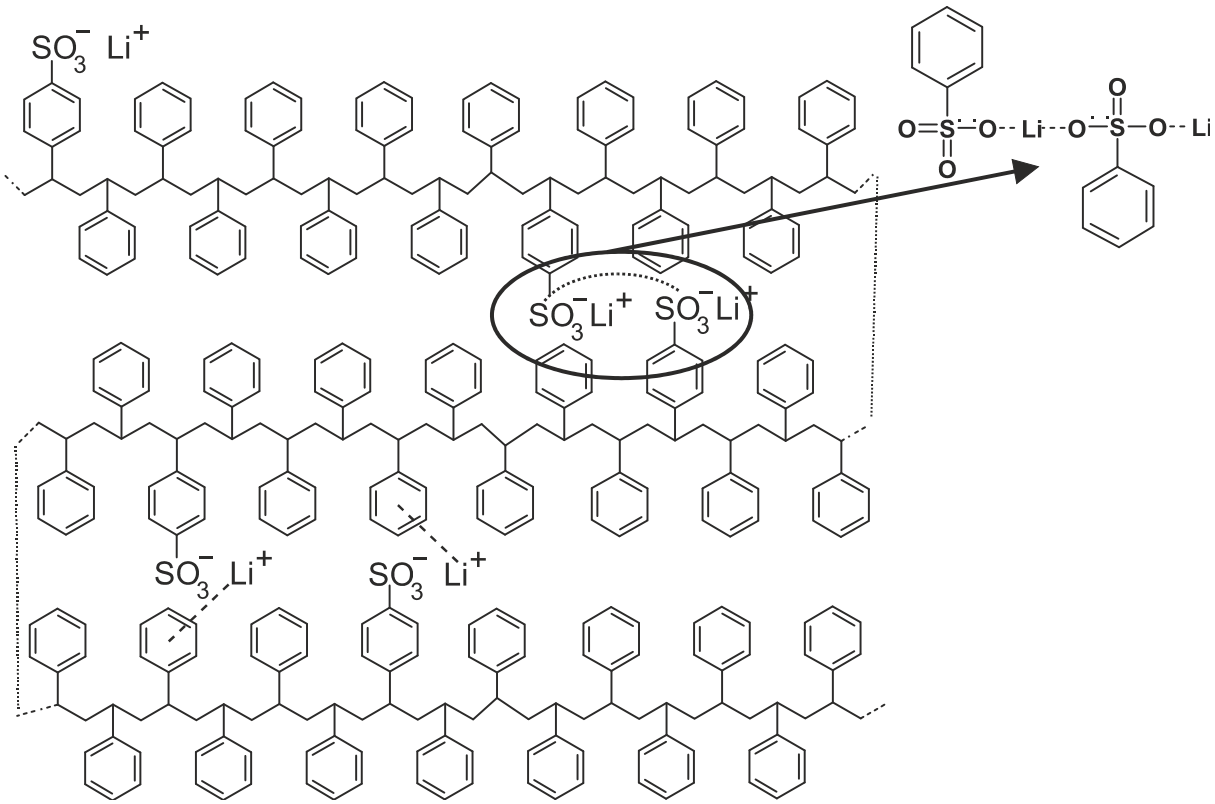

Fig. 6-14. Schematic illustration of possible complexation mechanisms in SPS neutralized with a monovalent counterion.

This type of complexation apparently leads to the SANS spectra that are not tractable with either Debye-Bueche, or two correlation lengths models. The latter, when least-squares fitted to the data, yields meaningless or unphysical values.

At this point we may speculate whether in the presence of polycarbonate the π-complexation changes so upon blending that it also involves the benzene rings of PC. Is it possible that we have a distribution of correlation lengths? An idea of such distributions can be encountered in the literature, e.g. in bimodal polymer gels [79].

6.5 Appendix. The upper critical solution temperature.

Spinodal curve separates a metastable region from an unstable region in the coexistence region of a binary mixture. On the Gibb's free energy of mixing curve vs. composition, $G_m(\varphi)$, the spinodal points are the zeros of the second derivative : $\frac{\partial^2 G_m}{\partial \varphi^2} = 0$. In real systems, fluctuations result in spinodal curve being not a sharp boundary.

Binodal curve defines the region of composition and temperature in a phase diagram for a binary mixture across which a transition occurs from miscibility of the components to conditions where single-phase mixtures are metastable or unstable. Binodal compositions are defined by pairs of points on the curve of Gibbs free energy of mixing vs. composition that have common tangents (Fig. 6-7). They correspond to compositions of equal chemical potentials of each of the two components in two phases (cf. e.g. [80]).

Upper Critical Solution Temperature (**UCST**) is the common maximum of spinodal and binodal curves (if both curves have maxima). If the common point of spinodal and binodal is the minimum of both, we speak of Lower Critical Solution Temperature (LCST).

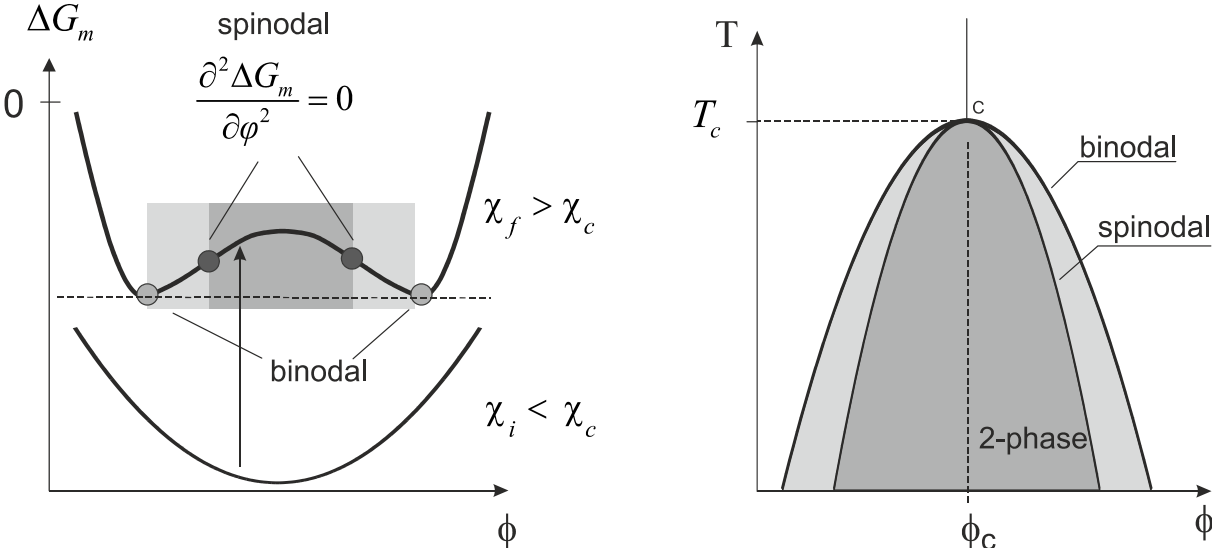

Fig. 6-15. Construction of the binodal and spinodal curves and the Upper Critical Solution Temperature point. Redrawn after a figure in [98].

A two component blend is miscible if and only if the following condition holds:

$$\left(\frac{\partial^2 \Delta G_{mix}}{\partial \varphi^2}\right)_{T,p} > 0, \tag{6.7}$$

where ΔG_{mix} is the Gibbs free energy of mixing and φ is the volume fraction of one component. One can calculate ΔG_{mix} from several theoretical models, of which the best known is Flory–Huggins theory [81].

7 Neutron polarization analysis in practical materials research problems

7.1 Introduction

Neutron scattering techniques are more and more often used in solving problems in applied sciences such as materials engineering. A good example here is the analysis of residual strains and stresses in bulk samples (e.g. parts of machinery), neutron reflectometry used the studies of materials for microelectronics, or investigation of large scale macromolecular structures via small angle scattering. In all cases use is being made of some unique properties of neutrons, namely:

- The refractive index for neutrons of a material against vacuum, $n \equiv \frac{k_1}{k_0} = 1 - \frac{\lambda^2 \rho}{2\pi}$ (ρ – is the scattering length density of the material) is less than 1, and therefore it implies "total external reflection" as opposed to total internal reflection one is used to e.g. lightguides. This is what neutron reflectometry (or grazing angle scattering) relies on.
- Neutrons are deeply penetrating particles, hence analysis of residual strains deep inside large samples is possible. The same principle makes neutron radiography possible.
- Small angle neutron scattering largely profits from isotopic substitution.

7.2 Residual strains in ceramic-elastomer composites

Residual strains and stresses are by no means restricted to polycrystalline metallic samples of interest to metallurgists, or e.g. aircraft turbine manufacturers. For example, they can also develop in complexes involving rigid porous ceramics ad soft matter fillers. The difference is that the latter type of internal strains are much more difficult to measure since due to lack of crystal structure in soft filler, typical diffraction techniques are of little use. X-ray analysis would access only the outer thin layer of material, where internal strains are usually relaxed. However, diffuse scattering of polarized neutrons proved successful in this case [18].

Diffuse scattering of polarized neutrons with polarization analysis was applied to study complexes of SiO_2 ceramics with poly(urea-urethane) elastomers. They are obtained via infiltration of

porous ceramics by elastomer prior to the curing at elevated temperature. The resulting material combines the hardness of a ceramic with elasticity of the polymer, and hence remains of broad interest to the industry. However, the useful properties of the composite are at risk from internal strains arising both from cooling the material and from the curing processes in the elastomer, which may lead to unwanted delamination at the pore walls or even cracking of the ceramic skeleton.

The poly(urea-urethane) elastomer is a copolymer composed of hard and soft segments:

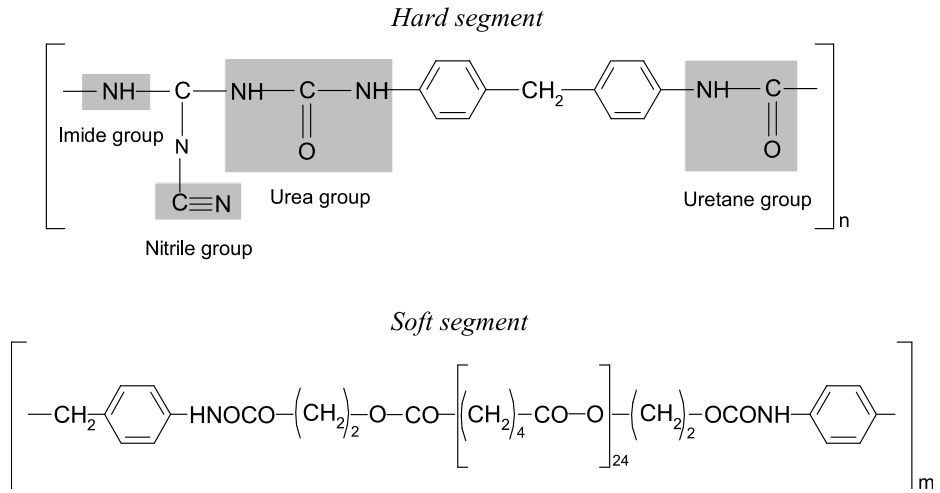

Fig. 7-1. Building units of poly(urea-urethane) elastomer.

In order to understand the possible correlations on microscopic lever, the structure of an isolated, unconstrained soft segment been simulated numerically. It appeared that the preferred arrangement of the chain was kind of a “twisted sheet” composed of helices as in Fig. 7-2 below.

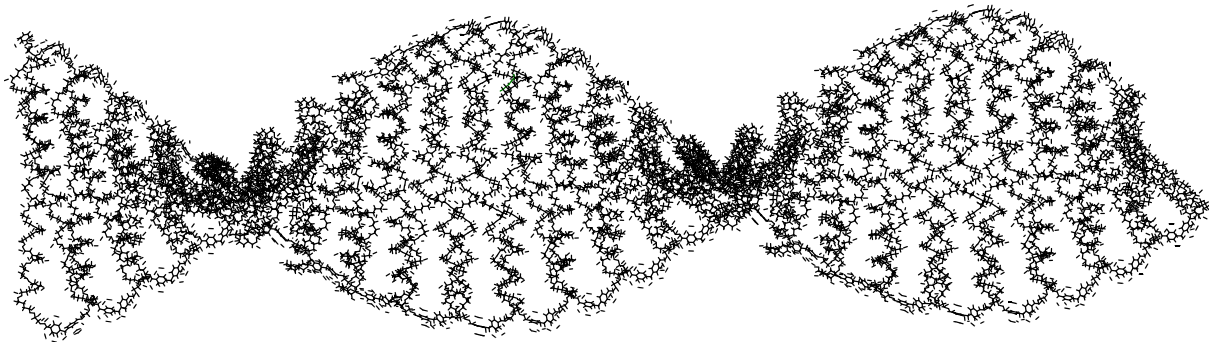

Fig. 7-2. "Twisted sheet" arrangement of an isolated soft segment. Energy-minimized computer simulation. Unpublished results.

Even though in a real elastomer, especially that confined in 50 or 70 μm pores, such an idealized structure never appears, the soft segments retain their piecewise-helical form, responsible for rubbery elasticity of the material:

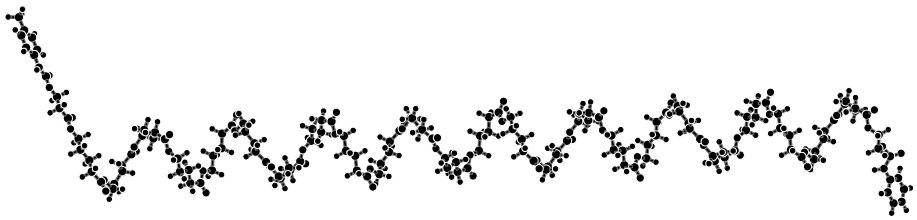

Fig. 7-3. Soft segment helix formed in a computer-simulated structure from fig. 7-2.

The pitch of such a helix is responsible for the coherent neutron scattering peak and thus its displacement could serve as the internal strain gauge. Indeed, if the peak position may be related to the corresponding real-space correlated distances in a semi-ordered matter through:

$$Q = \frac{2\pi}{d} \tag{7.1}$$

then very small changes in *d* result in coherent peak displacement:

$$\Delta Q = \frac{2\pi}{\Delta d}\,. \tag{7.2}$$

Two elastomers were used in this study of hard/soft segments ratios equal 0.25 and 1.5 and nicknamed PU125 and PU25, respectively. Diffuse scattering spectra for bulk samples of PU125 and PU25 measured with polarization analysis on the D7 instrument (ILL, Grenoble) are shown in Fig. 7-4. They contain peaks originating from highly correlated domains of hard segments as well as a tall peak, whose height compared with other peaks indicates that it comes from the phase being dominant in the sample, hence attributed to spatial correlations outside hard segment domains, whose position corresponds to the real space distance of 0.308±0.002nm, roughly the pitch of the helix shown in Fig. 7-3. Hard domains tend to develop crystalline

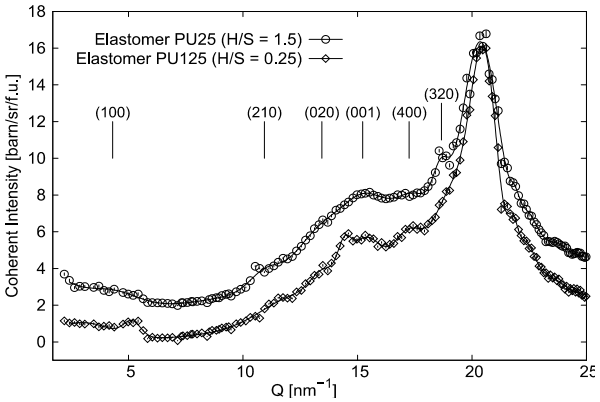

Fig. 7-4. Coherent neutron scattering spectra from bulk samples of PU125 and PU25 elastomers.

order due to interactions involving polar groups of short hard segments [82].

Both elastomers were then studied inside pores of two types of SiO_2 ceramic: the one with pore sizes of ca. 20 μm (denoted ceramic A) and the one with 70 μm pores (denoted ceramic B). Neutron coherent scattering spectra of elastomer PU25 inside type A ceramic and of PU125 inside type B ceramic are shown in Fig. 7-5. Displacement of the elastic segment peak is clearly seen and can be measured. It is attributed to the increase of 0.0063 ± 0.0028 nm in characteristic

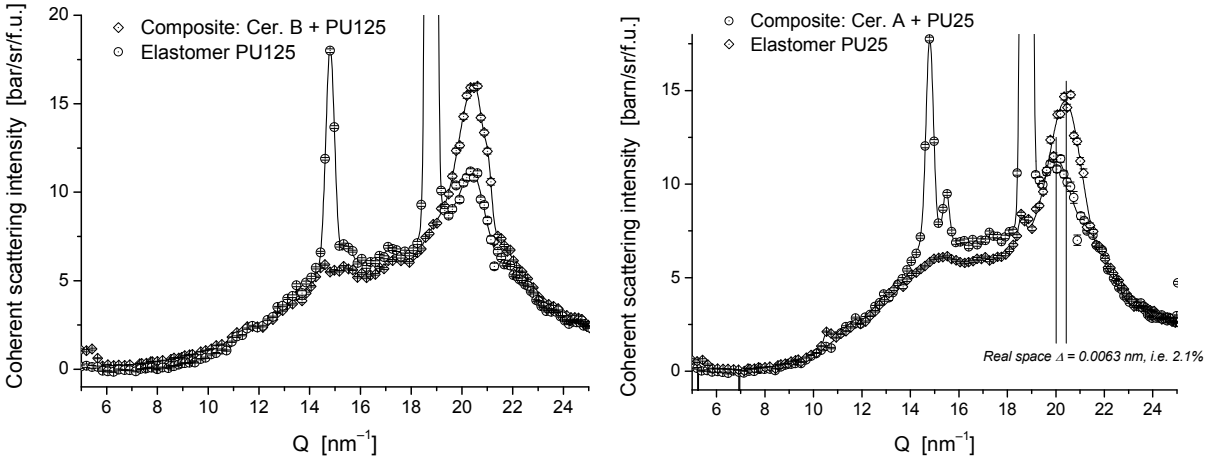

Fig. 7-5. Coherent neutron scattering from elastomer in porous ceramics as measured with polarized neutrons. Displacement of the elastic segment peak is a gauge of internal strain. [18]

correlation distance within the soft segment of the elastomer. This effect was observed in the composite of ceramic A with the PU25 elastomer only.

To the author's knowledge this is the only example known in literature of the application of diffuse scattering of polarized neutrons to the study of residual strains in soft matter.

7.3 Deducing from the coherent peak width

Research undertaken in course of the above work revealed that precise measurement of the coherent peak width in disordered soft matter may be a source of useful information of practical meaning. An interesting conclusion can be drawn out of comparison of the PU25 soft-segment peak width between composites of both ceramic types: A and B (Fig. 7-6).

Let us first recall a general principle. In a random structure where the *n*-th diffraction peak comes from the *n*-th nearest neighbours shell, if a given peak position corresponds to the mean distance $\langle a \rangle$ then its width ΔQ is related to the dispersion Δa of *a* through [37]:

$$\Delta Q = \frac{2\pi}{\langle a \rangle} \pi^2 n^2 \left(\frac{\Delta a}{\Delta Q} \right), \tag{7.3}$$

where *n* is the diffraction peak order. In this way ΔQ becomes and effective "measure of crystallinity". Moreover, detailed study of the *Q*-dependence of the peak width, supplemented with proper model calculations can classify a given structure as *paracrystalline* as opposed to affected by a mere distribution of correlation lengths [37].

Pores in type A ceramic are more than three times smaller than those in type B ceramic. The soft-segment peak is markedly broader in composite with type A ceramic demonstrating that, in this case the mean correlation distance is much shorter than in the other composite. The influence of mean pore size upon the correlation length is, however, indirect. Indeed, it can be easily estimated that, in the case shown in Fig. 7-6, the change in correlation length is three orders of magnitude smaller than the difference in pore sizes. Pore size must therefore influence rather the very domain structure of the elastomer and, through it, mean correlation lengths. The reason might be sought in surface-to-volume ratio being markedly greater in small pores, and hard segments engaged in hydrogen bond associations with hydroxyl groups available on the SiO_2 surface, are located next to this surface.

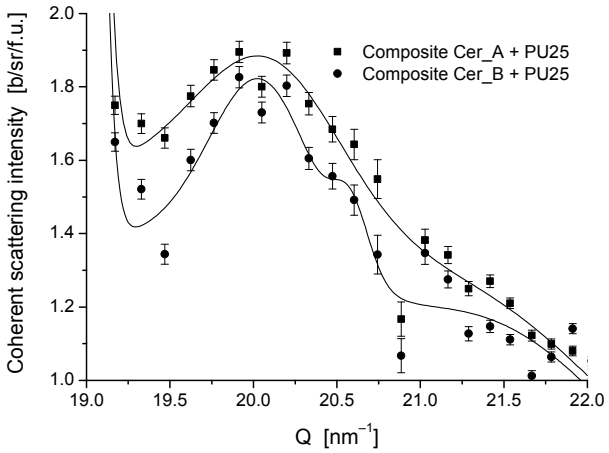

Fig. 7-6. Comparison of coherent peak widths of PU25 soft segments inside small (A-type) and large (B-type) pores. Unpublished data.

8 Atomic motions in the presence of various degrees of structural order

8.1 Inelastic scattering

In this chapter attention will be focused on inelastic scattering of thermal neutrons. Exchanging momentum end energy with atomic nuclei (nuclear scattering) or atomic spin systems (magnetic scattering) neutrons are an excellent measuring probe for molecular vibrations, including collective phenomena, or stochastic motions.

Fig. 8-1 provides a schematic overview of such motions (nuclear scattering only), accessible to inelastic neutron scattering techniques.

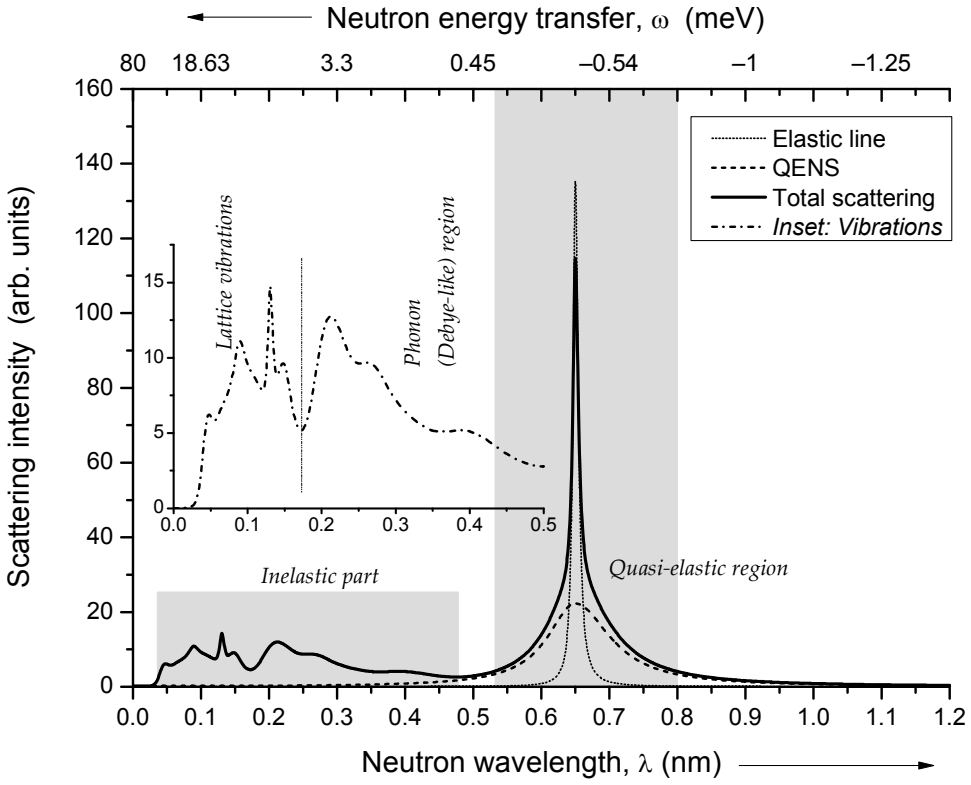

Fig. 8-1. "Anatomy" of a neutron inelastic scattering spectrum, showing elastic, quasi- and inelastic parts. Inset shows inelastic component in more detail.

For inelastic incoherent scattering, the intensity is proportional to the space and time Fourier transforms of the self-correlation function, $G_s(\mathbf{r},t)$, i.e. the probability of finding a particle at position **r** time *t* when the same particle was at $\mathbf{r}=0$ at $t=0$ [8,83]:

$$S_i(\mathbf{Q},\omega)=\frac{1}{2\pi\hbar}\iint G_s(\mathbf{r},t)e^{i(\mathbf{Q}\cdot\mathbf{r}-\omega t)}d\mathbf{r}dt \tag{8.1}$$

and:

$$G_s(\mathbf{r},t)=\frac{1}{N}\sum_j\int\left\langle\delta\left(\boldsymbol{\rho}-\mathbf{r}_j(0)\right)\delta\left(\boldsymbol{\rho}+\mathbf{r}-\mathbf{r}_j(t)\right)\right\rangle\, d\boldsymbol{\rho} \tag{8.2}$$

Inelastic incoherent neutron scattering is a very broad and highly explored field of research, using dedicated instruments and reach in voluminous literature. The scattering cross-section for phonon creation process at low temperatures can be written in the incoherent one-phonon scattering approximation in a commonly accepted notation (cf. [8,83]):

$$\sigma_{inc}(E_i,E_f,\phi,T)\approx\sqrt{\frac{E_f}{E_i}}\frac{\hbar\left|Q(E_i,E_f,\phi)\right|^2}{\omega}\sum_n\frac{\left(b_n^{inc}\right)^2}{M_n}\frac{\exp(-2W_n)}{1-\exp\left(\dfrac{-\hbar\omega}{k_BT}\right)}G(\omega), \tag{8.3}$$

where $Q(E_i,E_f,\varphi)$ is the neutron momentum transfer, $\omega=(E_i-E_f)$ is the neutron energy transfer, M_n is the mass of the *n*-th atom, and $\exp(-2W_n)$ is the Debye-Waller factor. The quantity being of interest in this type of experiments is $G(\omega)$, the so called atomic-displacement-weighted phonon or vibration density of states:

$$\begin{aligned}G(\omega)&=\sum_j\sum_n\left[A_j^n(\omega_j)\right]^2\delta(\omega-\omega_j),\quad\text{or:}\\ G(\omega)&=\sum_j\int d^3q\left[A_j^n(q)\right]^2\delta\left[\omega-\omega_j(q)\right]\end{aligned} \tag{8.4}$$

$G(\omega)$ may be seen as a projection of a family of dispersion curves upon the energy (vertical) axis. Being free from selection rules, it is a complementary technique to other vibrational spectroscopic methods, such as infrared or Raman. In molecular systems simpler than complex polymer structures, it is now routinely accompanied by *ab initio* calculations of vibrational states.

High resolution $\left(\Delta E / E \sim 2-3\%\right)$ incoherent inelastic neutron scattering spectra of polyisobutylene and cis-1,4 polyisoprene have been obtained on the TFXA spectrometer at the ISIS pulsed neutron scattering facility [84]. The observed bands were assigned with reference to available infrared and Raman data and the differences observed were discussed. Methyl group torsions were identified, which could not be observed with the optical techniques. These bands were significantly broadened compared to the instrumental resolution and this was attributed to a Gaussian distribution of local environment potentials for the methyl group.

8.2 Stochastic motions. Quasielastic neutron scattering.

Since we are now dealing with stochastic motions [85], there is no correlation between the positions of a given nucleus at $t=0$ and $t=\infty$. The space-Fourier transform of (8.2) gives the so called intermediate scattering function $I_{inc}\left(\mathbf{Q},t\right)$, which can be separated into its time-dependent and time-independent parts:

$$I_{inc}\left(\mathbf{Q},t\right)=I_{inc}\left(\mathbf{Q},\infty\right)+I'_{inc}\left(\mathbf{Q},t\right) \tag{8.5}$$

Taking both Fourier transforms gives:

$$I_{inc}\left(\mathbf{Q},\infty\right)=\frac{1}{N}\sum_{j}\left|\left\langle \exp\left(i\mathbf{Q}\cdot\mathbf{r}_{j}\right)\right\rangle\right|^{2} \tag{8.6}$$

and:

$$S_{inc}\left(\mathbf{Q},\omega\right)=I_{inc}\left(\mathbf{Q},\infty\right)\delta\left(\omega\right)+S_{inc}^{qel}\left(\mathbf{Q},\omega\right) \tag{8.7}$$

Elastic part of Eq. (8.7) (proportional to $\delta\left(\omega\right)$) vanishes for stochastic motions unrestricted in space, e.g. for linear (Brownian) diffusion. Spatial averaging results in the dependence of the scattering law on the modulus of **Q**. For a motion confined in space, $S_{inc}\left(Q,\omega\right)$ contains an elastic contribution, and for a simple rotation it takes the following form:

$$S_{inc}\left(Q,\omega\right)=A\left(Q\right)\delta\left(\omega\right)+\left[1-A\left(Q\right)\right]\mathrm{L}\left(\omega,\Gamma\right), \tag{8.8}$$

where $\mathrm{L}(\omega,\Gamma)$ is a Lorentzian with the full width at half maximum (FWHM) equal to Γ. $\mathrm{L}(\omega,\Gamma)$ arises as a Fourier transform of the following form of the time-dependent part of the intermediate scattering function:

$$I'_{inc}(Q,t) \propto \exp\left(-Q^2 \frac{t}{\tau}\right) \tag{8.9}$$

Here τ is the characteristic time of a given type of motion. E.g. for stochastic jumps over equidistant sites on a circle, this will be a mean residence time in one position.

It can be seen from Eq. (8.8) that $S_{inc}(Q,\omega)$ depends upon Q only through the amplitude $A(Q)$. Since the time characteristic of a motion under study is expressed by the line width, the spatial characteristic can be deduced from the so called Elastic Incoherent Structure Factor (EISF):

$$\mathrm{EISF}(Q) = \frac{I_{el}(Q)}{I_{el}(Q) + I_{qel}(Q)}, \tag{8.10}$$

where $I_{el}(Q)$ and $I_{qel}(Q)$ are the elastic and quasielastic scattering intensities, respectively. EISF(Q) (8.10) is therefore a very important quantity derived from the QENS experiment, and any perturbation to its dependence upon Q may affect the identification of the motion geometry. The most frequent source of such perturbation is the superposition of diffraction (Bragg) peak upon the elastic incoherent one. Central elastic peak (at $\omega = 0$) is in such a case a sum of elastic coherent and elastic incoherent components. In well-ordered materials the Bragg peaks are narrow in Q, and it is usually enough to exclude the corresponding scattering angles from consideration. On the other hand, modern neutron scattering instruments produce high quality data collected in a large number of points in the Q-space so that more options for analysis are available, especially when diffraction peaks contaminating the elastic incoherent intensity are broad. An example of such a situation is presented in Fig. 8-2 (lower graph, labelled 4BT at 250 K). The graph represents scattering intensity integrated over a close vicinity of the elastic peak for each of the QENS spectra taken at different wave-vector transfers (so called "elastic window scan"). The substance being studied was the smectic E phase of 4-butyl-4'-isothiocyanato-biphenyl (4BT in short). Diffraction peaks from the well-established smectic order of molecules

are clearly seen on top of a "clean" $I^{incoh.}_{elastic+QENS}(Q)$ dependency, and can be easily taken account of in further QENS data analysis, as suggested by the linear fit performed in "clean" regions.

Somewhat more difficult case is shown in upper graph of Fig. 8-2, labelled 6BT. This is the data obtained in the same way as before, this time for a rapidly cooled sample of 6-butyl-4'-isothiocyanatobiphenyl (6BT in short). Here almost the whole range of the wavevector transfer seems to be "contaminated" with coherent scattering rendering the estimation of EISF(Q) (8.10) difficult and less reliable.

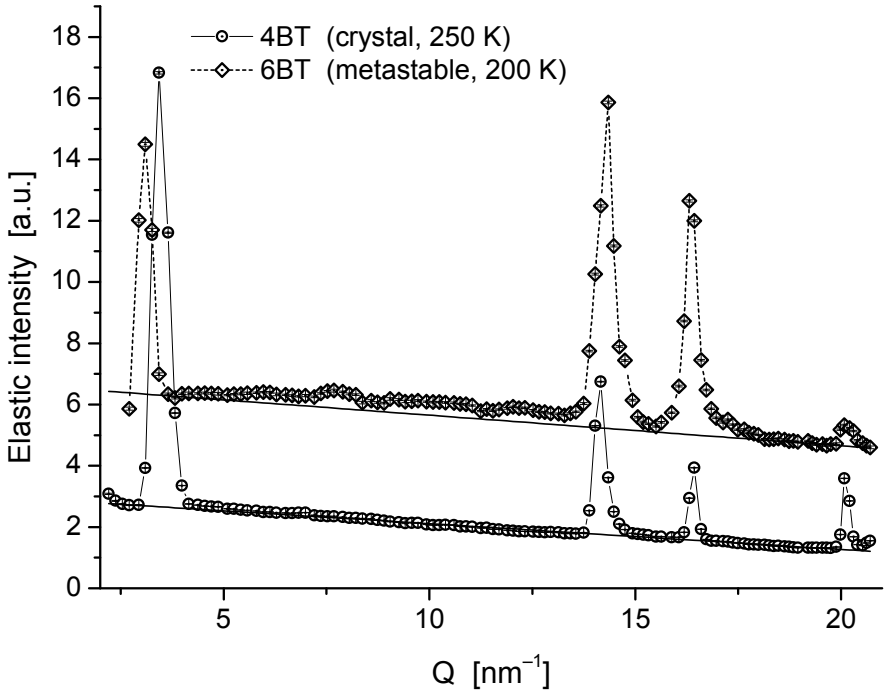

Fig. 8-2. Diffraction peaks over elastic incoherent intensity in QENS data of smectic E phase of 4-butyl-4'-isothiocyanato-biphenyl and 6-butyl-4'-isothiocyanatobiphenyl. ILL, Grenoble, instrument IN6. (E. Juszyńska, W. Zając, to be published.)

When studying stochastic motions in polymers, we are not quite as lucky as in the above example of 4BT, and even 6BT. Coherent intensity will usually make broad diffuse maxima that are intractable in a simple way, nor can the corresponding scattering angles be removed since almost nothing would be left. One can always argue that in hydrogen-rich samples with little coherent scattering the effect of coherent contamination is highly negligible. Indeed, in many cases this is true.

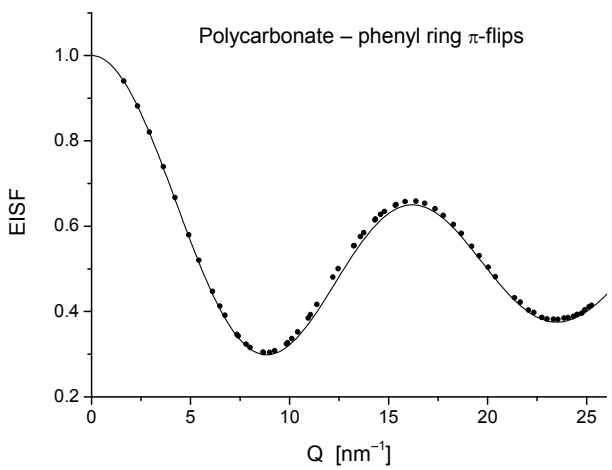

Fig. 8-3. Phenyl ring flips in polycarbonate. Calculated EISF with experimental coherent contamination.

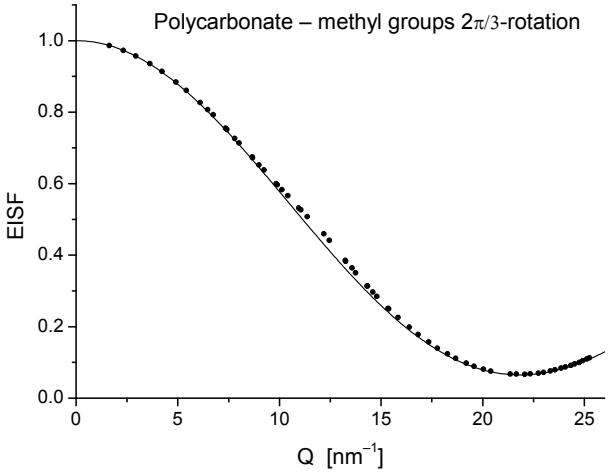

Fig. 8-4. Methyl group 120-deg. reorientation around C3 axis in polycarbonate. Calculated EISF with experimental coherent contamination.

Figs 8-3 and 8-4 illustrate this case, with polycarbonate as an example. Theoretical expressions for EISF in case of π-flips of the phenyl rings and jump-reorientation of CH_3 groups around their 3-fold axes were plotted. Black dots are would-be EISF values if coherent intensity added to elastic incoherent scattering. Coherent intensity measured on D7 instrument in barns per monomer per unit solid angle was used.

There are, however, cases, where without a method of separating coherent from incoherent scattering, no information on spatial characteristic of a motion can be deduced from the QENS experiment. A study of such a case has been presented in [86]. The material used was selectively deuterated syndiotactic poly(methyl metacrylate) (deuterated in α-methyl groups). This is an example of relatively large coherent cross section.

Selective deuteration is a procedure routinely used in QENS studies in order to focus attention on particular type of reorientation, involving hydrogen nuclei. Syndiotactic structure of the polymer adds to the short-range order, further enhancing coherent scattering intensity. Relative contribution to both types of scattering: coherent and incoherent are presented in Fig. 8-6.

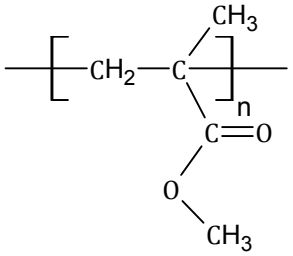

Fig. 8-5. PMMA building unit.

Fig. 8-7 shows the simulated effect that coherent contamination may have upon the elastic incoherent structure factor [86] in case syndiotactic partially deuterated PMMA.

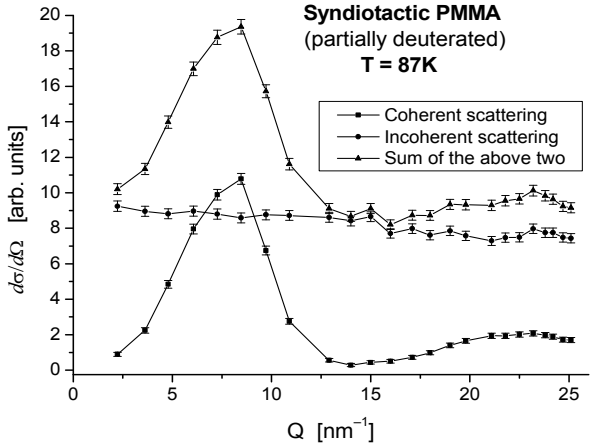

Fig. 8-6. The scattering spectrum of partially deuterated syndiotactic PMMA measured with polarization analysis. [86]

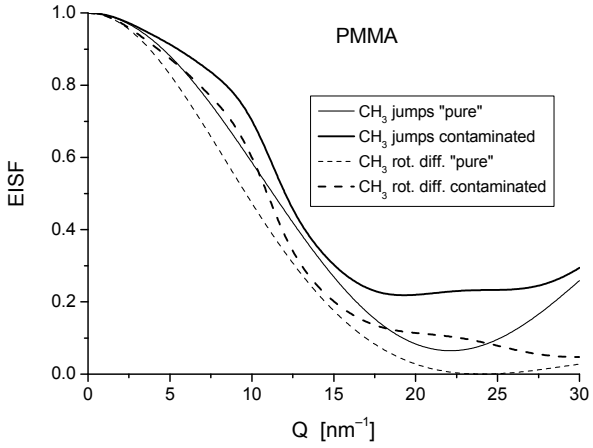

Fig. 8-8. Simulated influence of ''coherent contamination'' upon EISF(Q).

At this point one may feel tempted to proposing a QENS experiment with polarized neutrons with the aim to separate out incoherent scattering. In principle, such an experiment is possible on the D7 instrument at the ILL, operating in pulsed, time-of-flight mode. For that purpose the chopper is installed on the flightpath of incoming neutrons (cf. Fig. 3-1). However, test runs performed in time-of-flight set-up were quite discouraging due to extremely low counting rates achieved in particular time channels, and in fact, never published (Fig. 8-8).

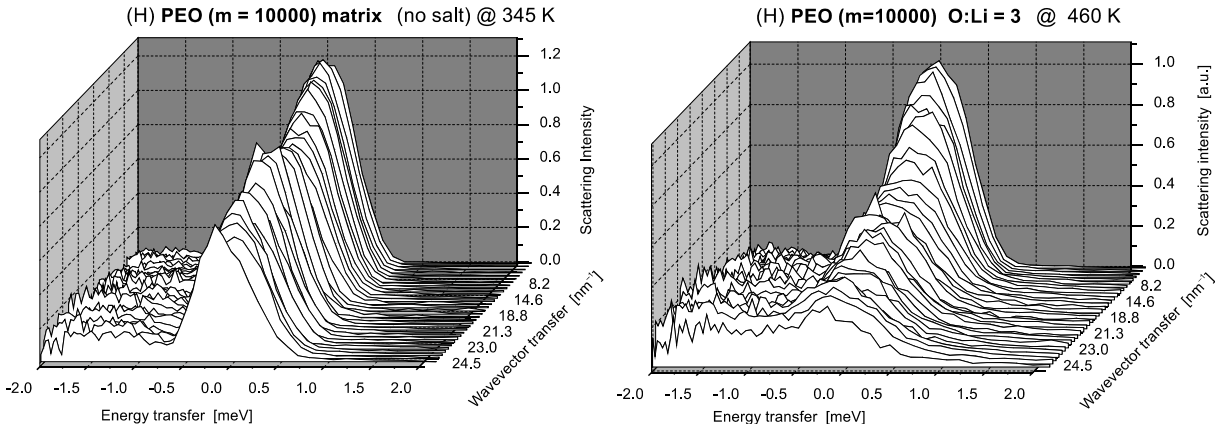

Fig. 8-7. QENS spectra of pure poly(ethylene oxide), PEO and a complex PEO · $LiClO_4$ obtained on the D7 instrument (ILL, Grenoble) operated in time-of-flight mode. Counting time for each sample: 12 hours. Neutron polarization analysis used to separate out incoherent scattering. (unpublished results)

Consequently, unreasonably long measuring times would have to be considered if meaningful counting statistics were to be attained. Significant improvements to the neutron optics may in future change this. Meanwhile, if dealing with partially disordered systems of significant diffuse scattering one has to follow an indirect path: first to measure coherent and incoherent components to the total scattering (as in Fig. 8-6) and use this information to correct the apparent EISF(Q) for the estimated coherent contamination.

9 Neutron scattering techniques less common with respect to short range order in soft matter

Neutron scattering techniques presented in this chapter are called "exotic" with respect to short range order in soft matter because they address rather specific issues and are rarely used due to their limited accessibility or because they are very demanding or beam time hungry. Here they are: (i) small angle scattering under zero average contrast condition (ZAC-SANS), and (ii) deep inelastic (Compton) scattering. Their proper use requires a well-defined physical problem (e.g. Compton scattering) and very much experimental time followed by a precise, method-specific calibration and detailed data analysis (ZAC-SANS).

9.1 Zero average contrast SANS

The concept of contrast match was introduced in Chapter 4. Now we are dealing with system composed of particles inhomogenous in terms of scattering length density. According to the principle of contrast match their average scattering length should be contrasted against that of the surrounding (e.g. solvent). However, if the very structure of the complex particles is being studied, then the opposite may be chosen, namely the surrounding (solvent) put at zero average contrast with respect to the particle.

A comprehensive description of his technique is given in [87].

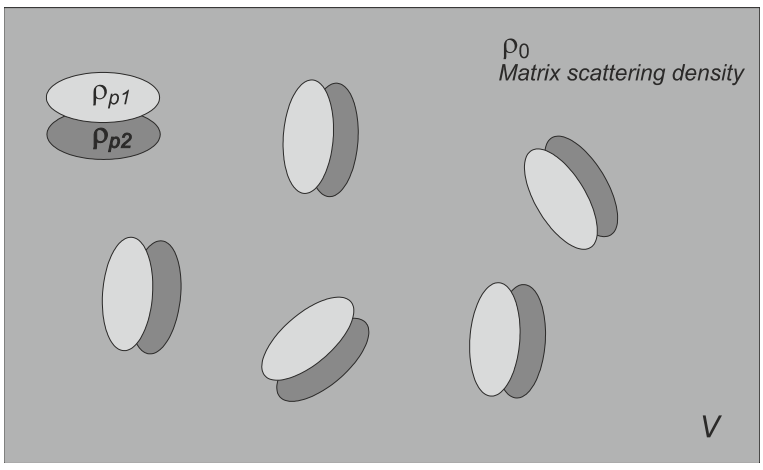

Fig. 9-1. The principle of the zero average contrast condition

SANS at zero average contrast condition was attempted as a method-of-choice to study self-organization phenomena in low molecular weight telechelic polystyrene zwitterions of general formula $R_1^- - \left[C_x H_y \cdots \right]_m - R_2^+$, namely [88] :

$$Br^- Me_3 N^+ - C_6 H_4 - \left[CH_2 CH\left(C_6 H_5\right) \right]_n - C\left(C_6 H_5\right)_2 - \left(CH_2\right)_3 - SO_3^- Li^+ ,$$

following a preliminary SANS analysis of this ionomer in solutions: in a non-polar solvent(toluene) and a polar one (cycohexanone) [89]. During this preliminary SANS study it became evident that zwitteionic polystyrene in both polar and non-polar solvents assumes far-from-simple structures, and that the aggregation processes are strongly concentration-dependent, rendering e.g. uninterpretable in a standard way, curved Zimm plots, and nonlinear Guinier plots.

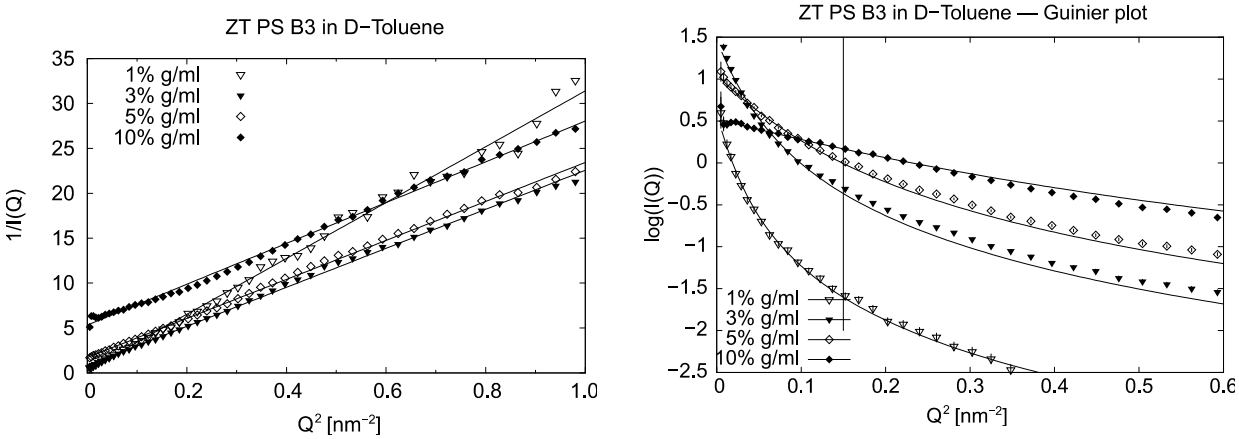

Fig. 9-2. Zimm (left) and Guinier plots of zwitterionic PS in deuterated toluene revealing concentration-dependent, complex mechanism of aggregation. [89]

Satisfactory fits to experimental data could only be achieved with the scattering law derived for fractal structures [43]:

$$\left(\frac{\partial \sigma}{\partial \Omega}\right)^{-1} \propto \left[1 + \frac{\left(D_f + 1\right)\left(Q\xi\right)^2}{3}\right]^{D_f/2}, \tag{9.1}$$

where D_f is the fractal dimension and ξ is a system-characteristic length scale. They are shown in (Fig. 9-4). The idea of attempting ZAC-SANS approach was triggered by the fact that zwitterionic PS was capable of creating complex spatial networks. These network were expected to be dependent upon polar properties of the solvent: in a polar solvent there should be ring-like

formations created by head-to-tail arrangement of zwitterions, while in a non-polar solvent ionic groups could aggregate, as shown in Fig. 9-3.

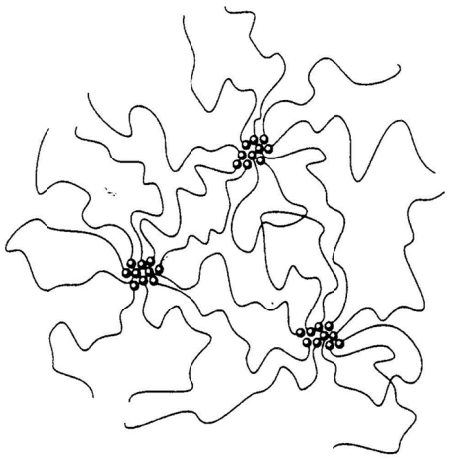

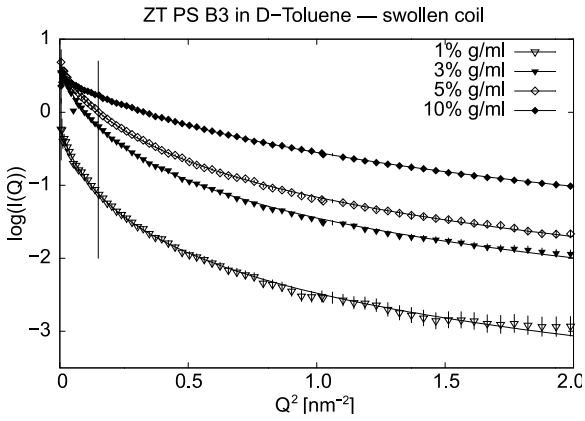

pe of
rent.

e

SANS under the zero average contrast condition (ZAC) makes it possible to decouple correlations due to polymer coil composition fluctuations from those due to polymer coil concentration fluctuations. During the ZAC-SANS experiment, the scattering intensity $I(Q)$ is considered to be a sum of intrachain $I_1(Q)$ and interchain $I_2(Q)$ parts. If the average scattering length varies within the chain, e.g. if $\overline{b_{cb}}$, the average scattering length of the chain body differs from $\overline{b_{eg}}$, the average scattering length of the end groups, then we may say:

$$I(Q) = I_1(Q) + I_2(Q) = \left[\left(N_{cb} \overline{b_{cb}} \right)^2 + \left(N_{eg} \overline{b_{eg}} \right)^2 \right] S_1(Q) + \left[N_{cb} \overline{b_{cb}} + N_{eg} \overline{b_{eg}} \right]^2 S_2(Q), \quad (9.2)$$

where N denotes the number density within the region of interest (cf. [90]). Under the zero average contrast condition only intraparticle correlations contribute to the scattering, since the average scattering length of the solvent may be tuned so that the second (interference) term in Eq. (9.2) effectively vanishes.

The measurements under the zero average contrast condition require extremely long counting time in order to collect reasonable statistics and because of this such experiments are a rarity on large scale neutron scattering facilities, where beam time is allocated on grounds of a scientific

merit of the proposal and feasibility of the proposed experiment. The proposal, under which this experiment was performed at the LOQ instrument at ISIS neutron source (Rutherford Appleton laboratory), was granted beam time, that was considered generous for a standard SANS experiment, but in case of ZAC measurements it allowed for a mere test of the method. In order to enhance intrachain correlations, partially deuterated sample with deuterated PS at the amine end was used (hereafter denoted the D-series of samples). Labels of D1, D2, etc. refer to different molecular weights, i.e.: D1: M_w = 6100, D2: M_w = 11500, D3: M_w = 26100, D4: M_w = 56700. The quality of data subjected to proper reduction and pre-processing operations, is illustrated in Fig. 9-5. Experimental results were analysed in terms of the Zimm plots (example shown in Fig. 9-6). Error bars are omitted from graphs in Fig. 9-6 as they would blur the plots considerably.

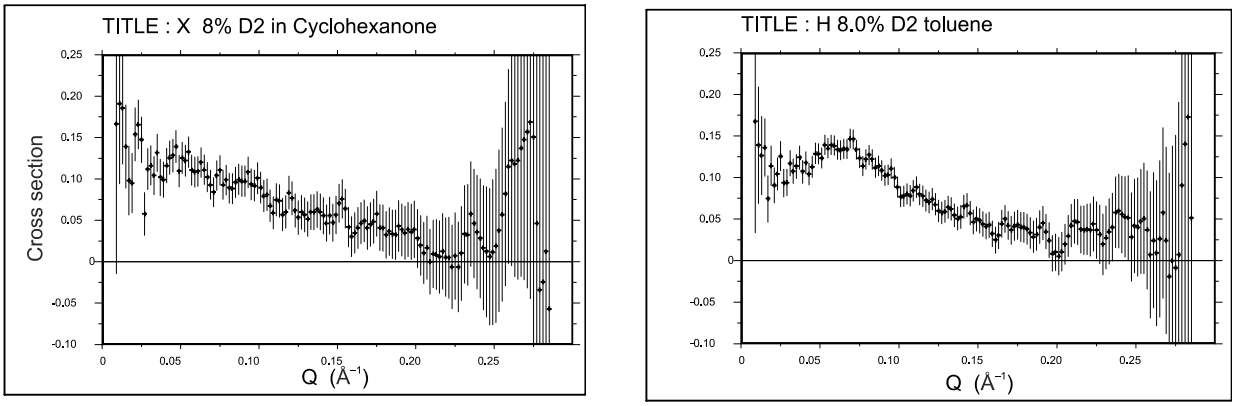

Fig. 9-5. Sample of SANS data for zwitterionic PS under ZAC, zero average contrast condition (proper mixture of hydrogenous and deuterated solvents ensured the ZAC).

Despite the low quality of data, some conclusions can be made. The chains of zwitterionic polystyrene aggregate, assuming internal structure od aggregates dependent upon the polarity of the solvent, although not in such a simple way, as expected. No evidence for ring-like arrangement of chains has been found.

SANS under zero average contrast condition is a very elegant but very challenging technique of addressing short range order phenomena in cases of intrachain correlations within respective ranges distances and object sizes.

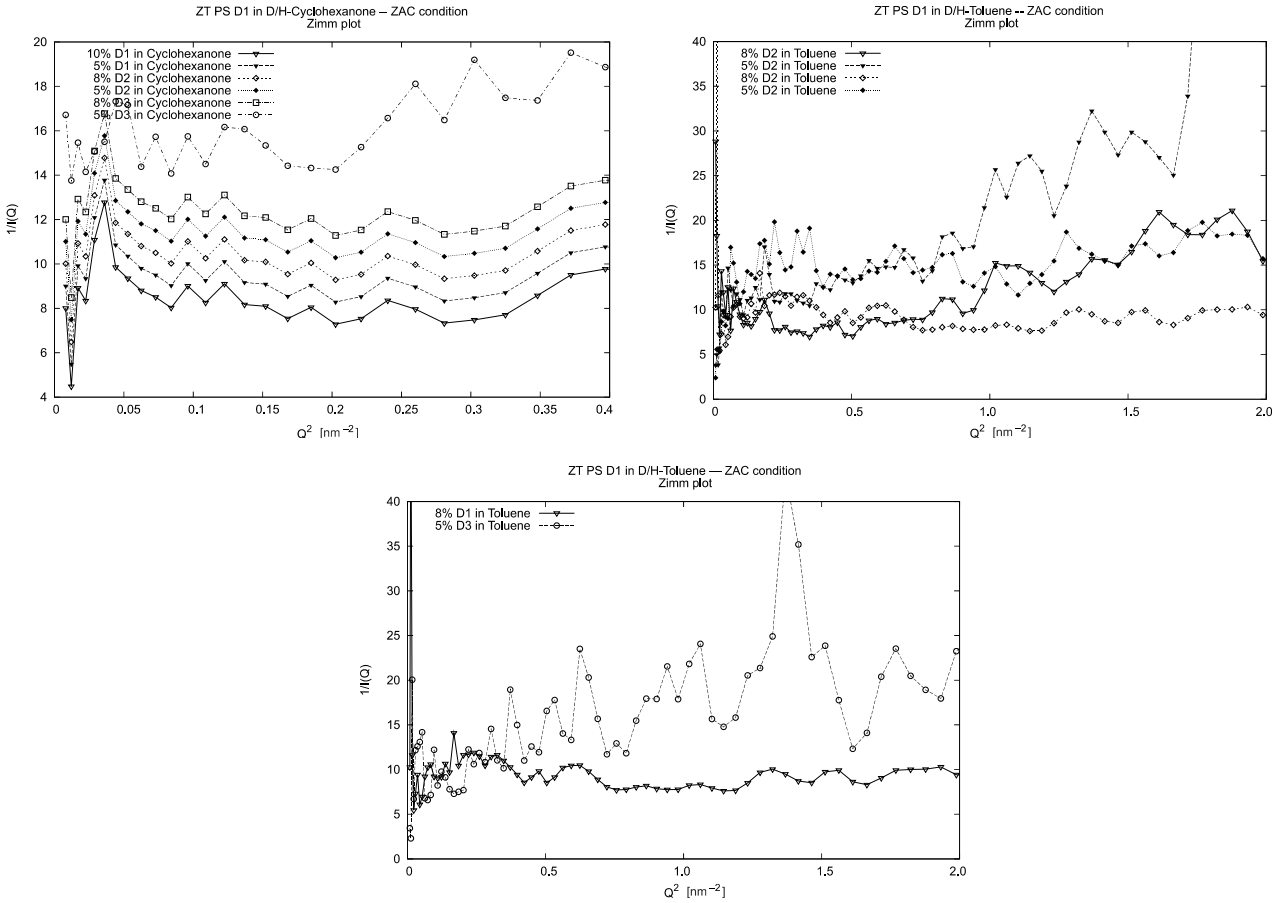

Fig. 9-6. Zimm plots generated from the SANS data of zwitterionic polystyrene under zero average contrast condition. Error bars omitted for clarity, original data quality to be assessed from the previous figure. Unpublished data.

9.2 Neutron deep inelastic (Compton) scattering

Deep inelastic (Compton) scattering is a neutron scattering technique, specific to pulsed sources, originally developed for studying quantum effects in matter [91-94]. It was first proposed in 1966 by Hohenberg and Platzman [95]. However, it may also be applied to certain structural problems in soft matter, whereby local atomic environment can be probed by measuring properties of kinetic energy of that atom [96]. Deep inelastic neutron scattering relies on the so called impulse approximation (IA), where the scattering cross section is simply related to the single-particle momentum distribution of atomic nuclei in the target. It requires neutrons of energies (much) greater than 1 eV, i.e. significantly higher than in other neutron scattering experiments probing condensed matter (cf. e.g. [93]).

In this experiment we measure an "effective" projection of nuclear momentum upon the direction of neutron momentum transfer, **q**. In neutron Compton scattering it is usually denoted by *Y*. The structure factor, $S(\mathbf{q},\omega)$, associated with the distribution of atomic momenta $n(\mathbf{p})$ for an isotropic sample is given by [92]:

$$S(Q,\omega)=\left(\frac{M}{q}\right)J(Y),\quad \text{where}\quad Y=\frac{M}{q}\left(\omega-\frac{Q^2}{2M}\right). \tag{9.3}$$

Here $J(Y)$ is a probability distribution such, that $J(Y)dY$ is a measure of probability that the given atom has a momentum component along **q**. This function is sometimes called the Compton profile.

The experiment is performed in the so called inverted geometry, and with large energy transfers, typically 1 – 100 eV.

The dynamic structure factor $S(\mathbf{q},\omega)$ is connected with the distribution $n(\mathbf{p})$ via:

$$S(\mathbf{q},\omega)=\frac{1}{h}\int n(\mathbf{p})\delta\left(h\omega-\frac{hq^2}{2M}-\frac{h\mathbf{p}\cdot\mathbf{q}}{M}\right)d^3p \tag{9.4}$$

If we chose the **z** direction so that it points along **q**, then (9.4) simplifies to:

$$S(q,\omega)=\frac{M}{hq}\int\delta\left(Y-hp_z\right)n(p)\,dp \tag{9.5}$$

and after integration:

$$S(q,\omega)=\left(\frac{M}{hq}\right)J(Y);\quad J(Y)=\int n(p_x,p_y,Y)\,dp_x dp_y \tag{9.6}$$

If:

$$Y=\left(\frac{M}{q}\right)\left(\omega-\frac{hq^2}{2M}\right) \tag{9.7}$$

then by measuring the neutron momentum transfer and the energy loss one can determine the projection of atomic momentum upon the direction of **q**. From the energy conservation we have:

$$E_k = \frac{(\mathbf{p}+\mathbf{q})^2 - p^2}{2M}, \tag{9.8}$$

where $(\mathbf{p}+\mathbf{q})$ is the final momentum of the neutron.

The method was applied to the sample of textured polyethylene [96]. The texture (preferred orientation of polymer chains) was introduced via high temperature stretching. Compton profiles were measured perpendicular to the texture direction (Fig. 9-7). The measured kinetic energies were in agreement with hose known from computer simulations. The results were promising: the method can add significant information to the analysis of vibrational states in directionally textured, or otherwise oriented material.

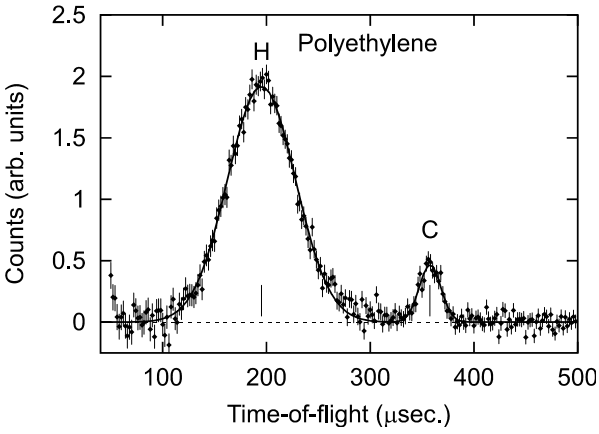

Fig. 9-7. Compton neutron scattering on textured polyethylene [96].

References:

[1] J. Chrusciel, W. Zajac, C. Carlile, Molecular Crystals and Liquid Crystals 262 (1995) 361 - 369.

[2] J. Chrusciel, W. Zając, Liquid Crystals 10 (1991) 419-424.

[3] R. Jakubas, J.A. Janik, J. Krawczyk, J. Mayer, I. Natkaniec, T. Stanek, O. Steinsvoll, W. Zając, Physica B: Condensed Matter 271 (1999) 309-314.

[4] S. Urban, W. Zajac, R. Jakubas, C. Carlile, B. Gabrys, Physica B: Condensed Matter 180-181 (1992) 1050-1052.

[5] W. Zając, S. Urban, V. Domenici, M. Geppi, C. Veracini, M. Telling, B. Gabryś, Physical Review E 73 (2006) 051704 - 051704-8.

[6] A. Serebrov, A. Fomin, Physical Review C 82 (2010).

[7] The NIST Reference On Constants, Units, and Uncertainty (n.d.).

[8] G.L. Squires, Introduction To the theory Of thermal Neutron Scattering , Dover Publications, Mineola, N.Y . , 1996.

[9] S.W. Lovesey, The Theory Of Neutron Scattering From Condensed Matter Volume II, Oxford University Press, USA, 1986.

[10] S.W. Lovesey, The Theory Of Neutron Scattering From Condensed Matter Volume I, Oxford University Press, 1986.

[11] A. Foderaro, The Elements Of Neutron Interaction Theory, The MIT Press, 1971.

[12] P. Roman, Advanced Quantum Theory, Addisn-Wesley Publishing Co., Reading, Massachusetts, 1965.

[13] A.-J. Dianoux, G. Lander, eds., Neutron Data Booklet, second ed., Institut Laue-Langevin, Grenoble, 2003, n.d.

[14] V. Sears, Neutron News 3 (1992) 26-37.

[15] R. Moon, T. Riste, W. Koehler, Physical Review 181 (1969) 920-931.

[16] O. Schärpf, (2010) 246.

[17] W. Zajac, B.J. Gabrys, O. Schärpf, K.H. Andersen, E.E. Parsonage, Solid State Ionics 147 (2002) 213-223.

[18] W. Zając, A. Boczkowska, K. Babski, K. Kurzydłowski, P. Deen, Acta Materialia 56 (2008) 5964-5971.

[19] W.G. Williams, Polarized Neutrons, Oxford University Press, Oxford, 1988.

[20] S.M. Shapiro, L. Passell, A. Zaliznyak, V.J. Ghosh, W.L. Leonhardt, M.E. Hagen, in:, Proceedings Of the 17th Meeting Of the International Collaboration On Advanced Neutron Source Santa Fe, New Mexico, April 25-29, 2005, 2005.

[21] O. Schärpf, D7 as Polarization analysis Instrument, Historical Perspective. D7 Millenium Workshop Report, 2007.

[22] A. Wildes, with K. Andersen, R. Cubitt, H. Humblot, D. Jullien, A. Petoukhov, F. Tasset, C. Schanzer, Shah V, Physica B: Condensed Matter 385-386 (2006) 1134-1137.

[23] E. Babcock, S. Mattauch, A. Ioffe, Nuclear Instruments and Methods In Physics Research Section A: Accelerators, Spectrometers, Detectors and Associated Equipment 625 (2011) 43-46.

[24] S. Parnell, E. Babcock, K. Nünighoff, M. Skoda, S. Boag, S. Masalovich, W. Chen, R. Georgii, J. Wild, C. Frost, Nuclear Instruments and Methods In Physics Research Section A: Accelerators, Spectrometers, Detectors and Associated Equipment 598 (2009) 774-778.

[25] D. Hughes, M. Burgy, Physical Review 81 (1951) 498-506.

[26] J.R. Stewart, P.P. Deen, K.H. Andersen, H. Schober, J.-F. Barthélémy, J.M. Hillier, A.P. Murani, T. Hayes, B. Lindenau, Journal Of Applied Crystallography 42 (2009) 69-84.

[27] M. Utsuro, V.K. Ignatovich, Handbook Of Neutron Optics, Wiley, 2010.

[28] B. Gabryś, O. Schärpf, Physica B: Condensed Matter 180-181 (1992) 495-498.

[29] O. Schärpf, B.J. Gabrys, D.G. Peiffer, ILL Report 90SC26T: Short-Range Order In Isotactic, Atactic and Sulfonated Polystyrene Measured By Polarized Neutrons (Parts A & B), Grenoble, 1990.

[30] D.F.R. Mildner, J.M. Carpenter, Acta Crystallographica Section A 33 (1977) 954-961.

[31] J. Dawidowski, F. Bermejo, J. Granada, Physical Review B 58 (1998) 706-715.

[32] J. Dawidowski, J. Granada, R. Mayer, G. Cuello, V. Gillette, M. Bellissentfunel, Physica B: Condensed Matter 203 (1994) 116-128.

[33] J. Mayers, A.L. Fielding, R. Senesi, Nuclear Instruments and Methods In Physics Research Section A: Accelerators, Spectrometers, Detectors and Associated Equipment 481 (2002) 454-463.

[34] G. Vineyard, Physical Review 96 (1954) 93-98.

[35] F.G. Bischoff, M.L. Yeater, W.E. Moore, Nuclear Science and Engineering 48 (1972) 266-280.

[36] I. Blech, B. Averbach, Physical Review 137 (1965) A1113-A1116.

[37] O. Schärpf, Neutron Scattering By Polymers Using Spin Polarized Neutrons With Polarization Analysis, 2008.

[38] V.F. Sears, Advances In Physics 24 (1975) 1-45.

[39] J. Copley, Computer Physics Communications 7 (1974) 289-317.

[40] M.W. Johnson, Discus: A Computer Program For the Calculation Of Multiple Scattering Effects In Inelastic Neutron Scattering Experiments., 1974.

[41] R. Zorn, Nuclear Instruments and Methods In Physics Research Section A: Accelerators, Spectrometers, Detectors and Associated Equipment 479 (2002) 568-584.

[42] L.A. Feigin, D.A. Svergun, Structure Analysis By Small-Angle X-Ray and Neutron Scattering, 1st ed., Plenum Press, New Yourk & London, 1987.

[43] S.M. King, in:, R.A. Pethrick, J.V. Dawkins (Eds.), Modern Techniques For Polymer Characterisation, John Wiley & Sons, 1999, p. 410.

[44] H.C. van de Hulst, Light Scattering By Small Particles, John Wiley & Sons, 1957.

[45] S. Schlick, ed., Ionomers: Characterization, Theory and Applications, CRC-Press, 1996.

[46] P.J. Flory, Principles Of Polymer Chemistry, Cornell University Press, 1953.

[47] P.J. Flory, Statistical Mechanics Of Chain Molecules, Interscience, 1969.

[48] P.J. Flory, The Journal Of Chemical Physics 17 (1949) 303.

[49] I. Iradi, F. Alvarez, J. Colmenero, A. Arbe, Physica B: Condensed Matter 350 (2004) E881-E884.

[50] M. Mondello, H.-J. Yang, H. Furuya, R.-J. Roe, Macromolecules 27 (1994) 3566-3574.

[51] K. Neumann, O. Schärpf, K. Ziebeck, Physica B: Condensed Matter 180-181 (1992) 817-818.

[52] B.K. Vainshtein, Diffraction Of X-rays By Chain Molecules, Elsevier Publishing Company, 1966.

[53] L.A. Utracki, ed., Polymer Blends Handbook, Springer - Verlag, 2002.

[54] M.S. Kalhoro, B.J. Gabrys, W. Zajac, S.M. King, D.G. Peiffer, Polymer 42 (2001) 1679-1690.

[55] L. Robeson, Polymer Blends: A Comprehensive Review, Hanser, Munich ;;Cincinnati, 2007.

[56] B.J. Gabryś, in:, S. Schlick (Ed.), Ionomers: Characterization, Theory, and Applications, CRC-Press, Boca Raton, 1996, p. 320.

[57] R. Tucker, B. Gabrys, W. Zajac, K.H. Andersen, M.S. Kalhoro, R.A. Weiss, in:, P. Cebe, D.J. Lohse, B.S. Hsiao (Eds.), Scattering From Polymers: Characterization By X-Rays, Neutrons, and Light (ACS Symposium Series, 739), American Chemical Society, 2000.

[58] V. Arrighi, W. Zajac, S. Shenoy, D. Martin Y Marero, B.J. Gabryś, M.T. Garay, S. Gagliardi, K.H. Andersen, Physica B: Condensed Matter 276-278 (2000) 849-851.

[59] B. Gabrys, W. Zajac, M.S. Kalhoro, K.H. Andersen, S.M. King, Physica B: Condensed Matter 276-278 (2000) 911-913.

[60] M. Rutkowska, A. Eisenberg, Macromolecules 17 (1984) 821-824.

[61] X. Lu, R.A. Weiss, Macromolecules 29 (1996) 1216-1221.

[62] X. Rui, R.A. Weiss, Polymer 39 (1998) 2851-2858.

[63] J. Eilhard, A. Zirkel, W. Tschöp, O. Hahn, K. Kremer, O. Schärpf, D. Richter, U. Buchenau, The Journal Of Chemical Physics 110 (1999) 1819.

[64] C. Lamers, O. Schärpf, W. Schweika, J. Batoulis, K. Sommer, D. Richter, Physica B: Condensed Matter 180-181 (1992) 515-518.

[65] LOQ - Small angle Neutron Scattering (SANS) {http://www.isis.stfc.ac.uk/instruments/loq/} (n.d.).

[66] R.K. Heenan, J. Penfold, S.M. King, Journal Of Applied Crystallography 30 (1997) 1140-1147.

[67] P. Debye, A.M. Bueche, Journal Of Applied Physics 20 (1949) 518.

[68] Y.W. Cheung, R.S. Stein, G.D. Wignall, H.E. Yang, Macromolecules 26 (1993) 5365-5371.

[69] J.S. Higgins, H.C. Benoit, Polymers and Neutron Scattering, Oxford University Press, Oxford, 1997.

[70] D.W.M. Marr, Macromolecules 28 (1995) 8470-8476.

[71] N. Tan, X. Liu, R. Briber, D.G. Peiffer, Polymer 36 (1995) 1969-1973.

[72] M. Moritani, T. Inoue, M. Motegi, H. Kawai, Macromolecules 3 (1970) 433-441.

[73] L.K. Nicholson, K. Mahmood, B.J. Gabrys, D. Vesely, D.G. Peiffer, Polymer 40 (1999) 6099-6111.

[74] G.C. Gemeinhardt, R.B. Moore, Macromolecules 38 (2005) 2813-2819.

[75] W. Zając, B.J. Gabryś, Phase Transitions 80 (2007) 501-509.

[76] N.C. Zhou, W.R. Burghardt, K.I. Winey, Macromolecules 40 (2007) 6401-6405.

[77] A.J. Ro, S.J. Huang, R.A. Weiss, Polymer 50 (2009) 1134-1143.

[78] M.D. Ossowska-Chruściel, Private Communication, n.d.

[79] A.-M. Hecht, F. Horkay, E. Geissler, The Journal Of Physical Chemistry B 105 (2001) 5637-5642.

[80] J.S. Higgins, J.E.G. Lipson, R.P. White, Philosophical Transactions. Series A, Mathematical, Physical, and Engineering Sciences 368 (2010) 1009-25.

[81] P.J. Flory, The Journal Of Chemical Physics 9 (1941) 660.

[82] J. Blackwell, M. Ross, Journal Of Polymer Science: Polymer Letters Edition 17 (1979) 447-451.

[83] W. Marshall, S.W. Lovesey, Theory Of thermal Neutron Scattering: The Use Of Neutrons For the Investigation Of Condensed Matter, Clarendon Press, Oxford, 1971.

[84] M.A. Adams, B.J. Gabrys, W.M. Zajac, D.G. Peiffer, Macromolecules 38 (2005) 160-166.

[85] M. Bée, Quasielastic Neutron Scattering: Principles and applications In Solid State Chemistry, Biology and Materials Science, Adam Hilger, Bristol, UK, 1988.

[86] B. Gabrys, W. Zajac, O. Schärpf, Physica B: Condensed Matter 301 (2001) 69-77.

[87] M. Benmouna, B. Hammouda, Progress In Polymer Science 22 (1997) 49–92.

[88] W. Zając, B.J. Gabryś, J. Xu, D.G. Bucknall, R.W. Richards, in:, J. Chruściel (Ed.), Neutron Scattering and Complementary Methods In Investigations Of Condensed Phase, University of Podlasie, Siedlce, 2003, p. 156.

[89] W. Zając, B.J. Gabryś, D.G. Bucknall, J. Xu, R.W. Richards, L. Hutchings, Physica B: Condensed Matter 350 (2004) E975-E977.

[90] K. Nishida, H. Urakawa, K. Kaji, B. Gabrys, J. Higgins, Polymer 38 (1997) 6083-6085.

[91] R. Silver, Physical Review B 38 (1988) 2283-2296.

[92] J. Mayers, A.C. Evans, Measurement Of Atomic Momentum Distributions By Neutron Compton Scattering. Report RAL-91-048, Didcot, 1991.

[93] J. Mayers, Physical Review B 41 (1990) 41-51.

[94] J. Blostein, J. Dawidowski, J. Granada, Physical Review B 71 (2005) 054105-1 - 054105-12.

[95] P. Hohenberg, P. Platzman, Physical Review 152 (1966) 198-200.

[96] B.J. Gabrys, W. Zajac, J. Mayers, M.S. Kalhoro, Applied Physics A: Materials Science & Processing 74 (2002) s1645-s1647.

[97] Macrogalleria - the award-winning and Internationally Recognized Source Of Information In Polymer Science. {http://pslc.ws/macrogcss/} (n.d.).

[98] W. Köhler, Home Page: {http://www.ep4.phy.uni-bayreuth.de/ag_koehler/research/spinodal/spinodal.html}, Last accessed 12.03.2007 (n.d.).

PRINTED AT
THE HENRYK NIEWODNICZAŃSKI
INSTITUTE OF NUCLEAR PHYSICS
POLISH ACADEMY OF SCIENCES
KRAKÓW, POLAND

Xerocopy: IFJ PAN Kraków